Journal of Medicinal Chemistry

Article

Aminothiazoles as potent and selective Sirt2 inhibitors – a structure-activity relationship study

Matthias Schiedel, Tobias Rumpf, Berin Karaman, Attila Lehotzky, Judit Oláh, Stefan Gerhardt, Judit Ovádi, Wolfgang Sippl, Oliver Einsle, and Manfred Jung

J. Med. Chem., **Just Accepted Manuscript** • DOI: 10.1021/acs.jmedchem.5b01517 • Publication Date (Web): 22 Dec 2015

Aminothiazoles as potent and selective Sirt2 inhibitors – a structure-activity relationship study

Matthias Schiedel,[†] *Tobias Rumpf,*[†] *Berin Karaman,*[#] *Attila Lehotzky,*[§] *Judit Oláh,*[§] *Stefan Gerhardt,*[‖] *Judit Ovádi,*[§] *Wolfgang Sippl,*[#] *Oliver Einsle,*[‖] *Manfred Jung*[†]*

† Institute of Pharmaceutical Sciences, Albert-Ludwigs-University Freiburg, Albertstraße 25, 79104 Freiburg im Breisgau, Germany

Institute of Pharmacy, Martin-Luther-University Halle-Wittenberg, Wolfgang-Langenbeck-Straße 4, 06120 Halle (Saale), Germany

§ Institute of Enzymology, Research Centre for Natural Sciences, Hungarian Academy of Sciences, Magyar Tudósok körútja 2, H 1117 Budapest, Hungary

‖ Institute of Biochemistry and BIOSS Centre for Biological Signalling Studies, Albert-Ludwigs-University Freiburg, Albertstraße 21, 79104 Freiburg im Breisgau, Germany

KEYWORDS: epigenetics, histone deacetylases, sirtuins, inhibitors, drug design

ABSTRACT: Sirtuins are NAD^+-dependent protein deacylases that cleave off acetyl, but also other acyl groups from the ε-amino group of lysines in histones and other substrate proteins. Dysregulation of human Sirt2 (hSirt2) activity has been associated with the pathogenesis of cancer, inflammation, and neurodegeneration, which makes the modulation of hSirt2 activity a promising strategy for pharmaceutical intervention. The Sirtuin Rearranging Ligands (SirReals) have recently been discovered by us as highly potent and isotype-selective hSirt2 inhibitors. Here, we present a well-defined structure-activity relationship study, which rationalizes the unique features of the SirReals and probes the limits of modifications on this scaffold regarding inhibitor potency. Moreover, we present a crystal structure of hSirt2 in complex with an optimized SirReal derivative that exhibits an improved *in vitro* activity. Lastly, we show cellular hyperacetylation of the hSirt2 targeted tubulin caused by our improved lead structure.

INTRODUCTION: Until today, 18 different histone deacetylases (HDACs) have been identified and grouped into four classes, according to their homology to yeast HDACs, which were the first to be discovered.[1] Class I, II, and IV HDACs are Zn^{2+}-dependent, while sirtuins, initially described as class III HDACs or Sir2 proteins, constitute a unique class of this enzyme super family. Sirtuins are dependent on NAD^+ as a cofactor to remove acetyl,[2] but also other acyl groups, such as myristoyl,[3] palmitoyl,[4] and succinyl,[5] from the ε-amino group of lysines. Beyond histones, a multitude of non-histone substrates has been identified in recent years, e.g. α-tubulin,[6] NFκB,[7] p53,[8] and BubR1.[9] Apart from deacylation, sirtuins were shown to catalyze ADP-ribosylation as well.[10] By regulating the acylation or ADP-ribosylation state of their substrate proteins, sirtuins have been implicated to influence a wide range of cellular processes like ageing,[11] metabolic sensing, apoptosis,[12] inflammation,[13] and transcription.[14] Sirtuins have been conserved from bacteria to eukaryotes and share a catalytic domain of approximately 260 amino acids with a high degree of sequence similarity. While bacteria and archaebacteria possess only one or two sirtuins, in eukaryotes this number is higher. The human genome encodes seven sirtuin isotypes, which differ in their catalytic activity and their subcellular localization.[15] The human isotype Sirtuin 2 (hSirt2) is predominantly localized in the cytoplasm, however, it has also been found in the nucleus. hSirt2 was shown to have a major impact on cell cycle regulation,[6] peripheral myelination,[16] autophagy,[17] and immune and inflammatory response.[18] A dysregulation of hSirt2 activity was reported to play a critical role in the pathogenesis of cancer,[19] neurodegenerative diseases,[20] type II diabetes,[21] and bacterial infections.[18b, 18c] To further investigate the effects of hSirt2-dependent deacylation, and its impact on downstream signaling, modulators of hSirt2 activity are urgently needed. A number of hSirt2 modulators have been discovered thus far, and selected examples are depicted in Figure 1: the physiological

sirtuin inhibitor nicotinamide (**1**)[22] and its derivatives 5-((5-benzamidonaphthalen-1-yl)oxy)nicotinamide (**2**)[23] and the 3′-phenethyloxy-2-anilinobenzamide analogue **3**,[24] the highly potent but unselective ELT inhibitor 31 (**4**),[25] the highly selective 5,6,7,8-tetrahydrobenzo[4,5]thieno[2,3-d]pyrimidin-4(3H)-one (**5**),[26] AGK2 (**6**),[27] salermide (**7**),[28] and the macrocyclic peptide S2iL5 (**8**).[29] However, isotype-selective and drug-like inhibitors of hSirt2 with proven cellular activity are still scarce. Recently, we discovered a novel class of potent and highly isotype-selective hSirt2 inhibitors.[30] Due to a major rearrangement of the active site of hSirt2 upon ligand binding, these inhibitors were termed Sirtuin Rearranging Ligands (SirReals). The core of the SirReals is an acylated 2-aminothiazole scaffold, which connects an arylmethyl moiety with a 4,6-dimethylpyrimidine (Figure 1).

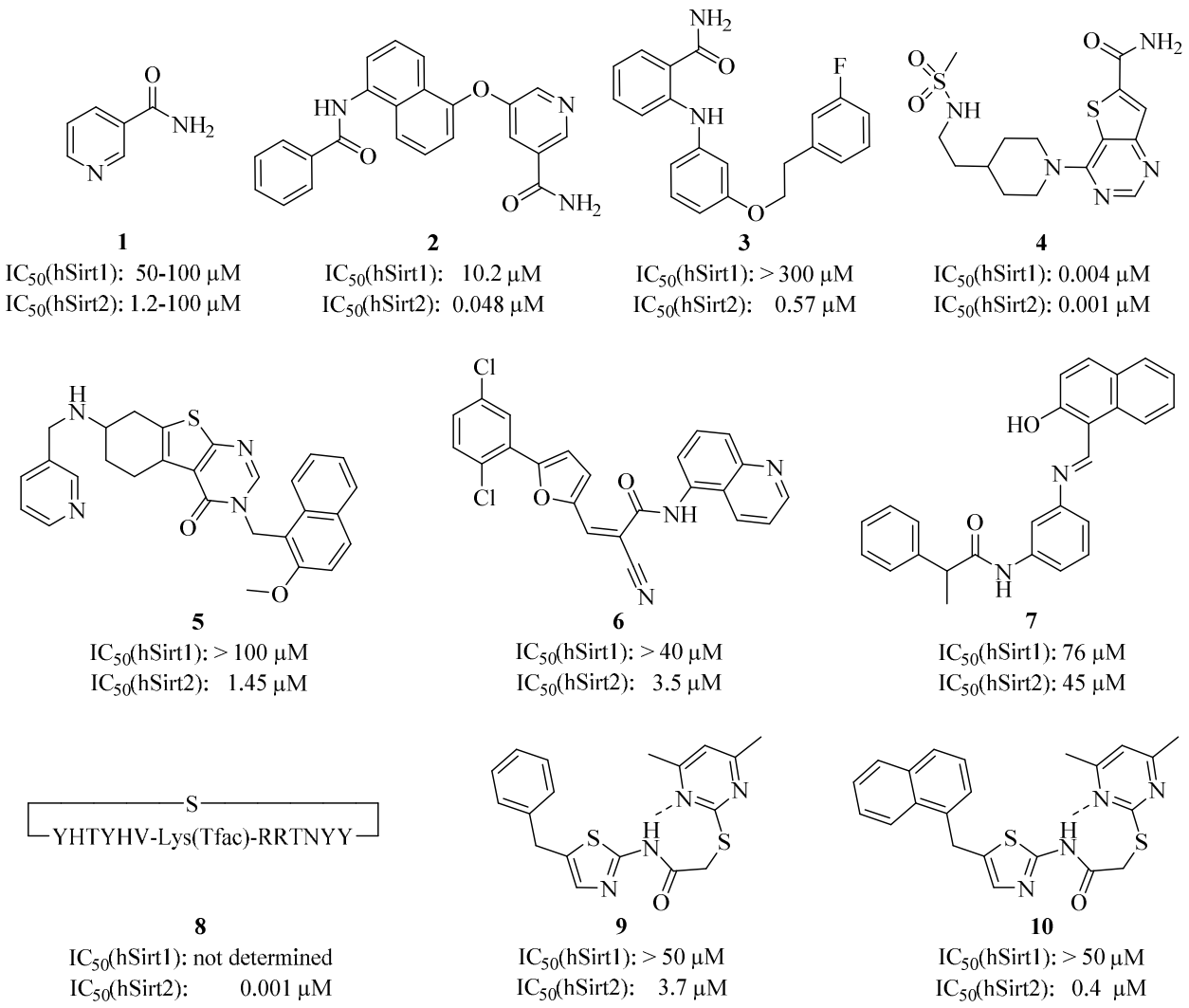

Figure 1. Chemical structures and inhibition data of selected hSirt2 inhibitors, including SirReal1 (**9**) and SirReal2 (**10**). The intramolecular hydrogen bonds are shown as dashed lines.

By inducing a rearrangement of the active site of hSirt2, the 4,6-dimethylpyrimidine moiety is bound to a yet-unexploited binding pocket, which lays the foundation for the excellent isotype-selectivity of the SirReals. Therefore, we named the newly formed binding site 'selectivity pocket'. The arylmethyl moiety protrudes towards the substrate channel pushing the acyl-lysine out of its physiological position, and thereby enlarging the distance between substrate and NAD^+. This efficiently blocks the acyl transfer. A preliminary structure activity relationship

(SAR) study has already been reported,[30] revealing an additive contribution of the arylmethyl and the 4,6-dimethylpyrimidine moiety, and the importance of the intramolecular hydrogen bond for activity. Here, we systematically probe further SARs to analyze the limits of modification within this scaffold.

RESULTS: Guided by the structural insights obtained from hSirt2-SirReal complexes,[30] we aimed to systematically probe the limits of variation within the scaffold of the SirReals and to established a well-defined SAR-model. To study the effect of an alteration of the aminothiazole core, we initially generated a few synthetically easily accessible aminothiadiazole derivatives. The synthesis of these inhibitors is outlined in Scheme 1. A condensation of a carboxylic acid and thiosemicarbazide yielded the aminothiadiazoles **11a-e**,[31] which were subsequently chloroacetylated to obtain **12a-g**.[32] A reaction of the alkyl chlorides with aromatic thiols generated the desired aminothiadiazoles **13a-h** (Table 1).

Scheme 1. Synthesis of aminothiadiazoles[a]

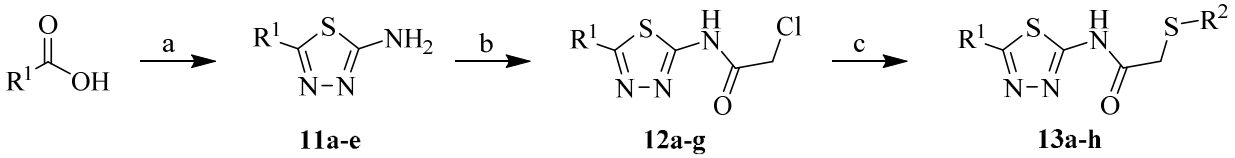

[a]Reagents and conditions: (a) thiosemicarbazide, H_2SO_4, 80 - 90 °C, 7 h; (b) acetyl chloride, DIPEA, acetonitrile, 0 °C to rt, 2 h; (c) aromatic thiol, Na_2CO_3, KI, DMSO, 2 h.

Our main focus was placed on the modifications of the arylmethyl and pyrimidine moieties, which were shown to be crucial for the interaction with the cofactor or ligand binding, respectively.[30] First, we explored modifications of the arylmethyl moiety. Molecular docking studies, based on the hSirt2-SirReal complexes,[30] indicated that substitutions at the naphthyl group of the parent compound **10** are beneficial for the potency of the ligands. Compound **14a**

(Figure 2a), a chloro-substituted derivative of the parent compound **10**, was predicted to interact with the two backbone carbonyl groups of His187 and Val233 (Figure 2b). By means of a halogenation of the naphthyl residue, we aimed to gain ligand affinity via a σ-hole interaction with the peptide backbone. To follow up on this hypothesis we synthesized the halogenated naphthyl derivatives **14a, 14d, 14f, 14g, 14i** (Table 2). Additionally, novel derivatives of the parent compound **9,** with substituted benzyl moieties, were generated to consider the impact of further structural changes of the arylmethyl moiety, as well. Encouraged by molecular docking studies, that showed a high docking score for the (*S*)-enantiomer of **14b** (Figure 2a,c), we aimed to synthesize SirReals with an additional alkylation in α-position to the carbonyl of the amide and eventually separated the enantiomers by chiral HPLC. The docking revealed that the methyl group ((*S*)-configuration) is orientated towards the exit of the selectivity pocket, which can accommodate longer alkyl groups. On the other hand, the (*R*)-configuration was predicted to be less favorable due to the close proximity of the conserved water molecule and Ile93. This is also reflected in the less favorable binding energies calculated for the (*R*)-enantiomer (Table S1). Furthermore, we wanted to investigate the effects of structural changes of different substitution patterns of the pyrimidine moiety. Initial structural data and SAR studies have shown that the 4,6-dimethylpyrimidine moiety perfectly fits into the newly formed 'selectivity pocket', and that a loss of the methyl groups leads to a decay in ligand potency.[30] Additionally, molecular docking, based on hSirt2-SirReal complexes,[30] demonstrated by the example of **14c** (Figure 2a), that larger alkyl substituents, e.g. ethyl, in position 4 and 6 of the pyrimidine moiety cause a steric clash with residues Ala135, Tyr139, and Leu206 of the 'selectivity pocket', as well as with Thr171 of the C-pocket. These studies predicted a loss of the H-bond to the conserved water molecule, and thereby lowering the ligand affinity to hSirt2 (Figure 2d). To show the accuracy of

our docking studies we still wanted to actually test, whether hSirt2 would be able to accommodate its 'selectivity pocket' to other substitution patterns of the pyrimidine moiety, as well.

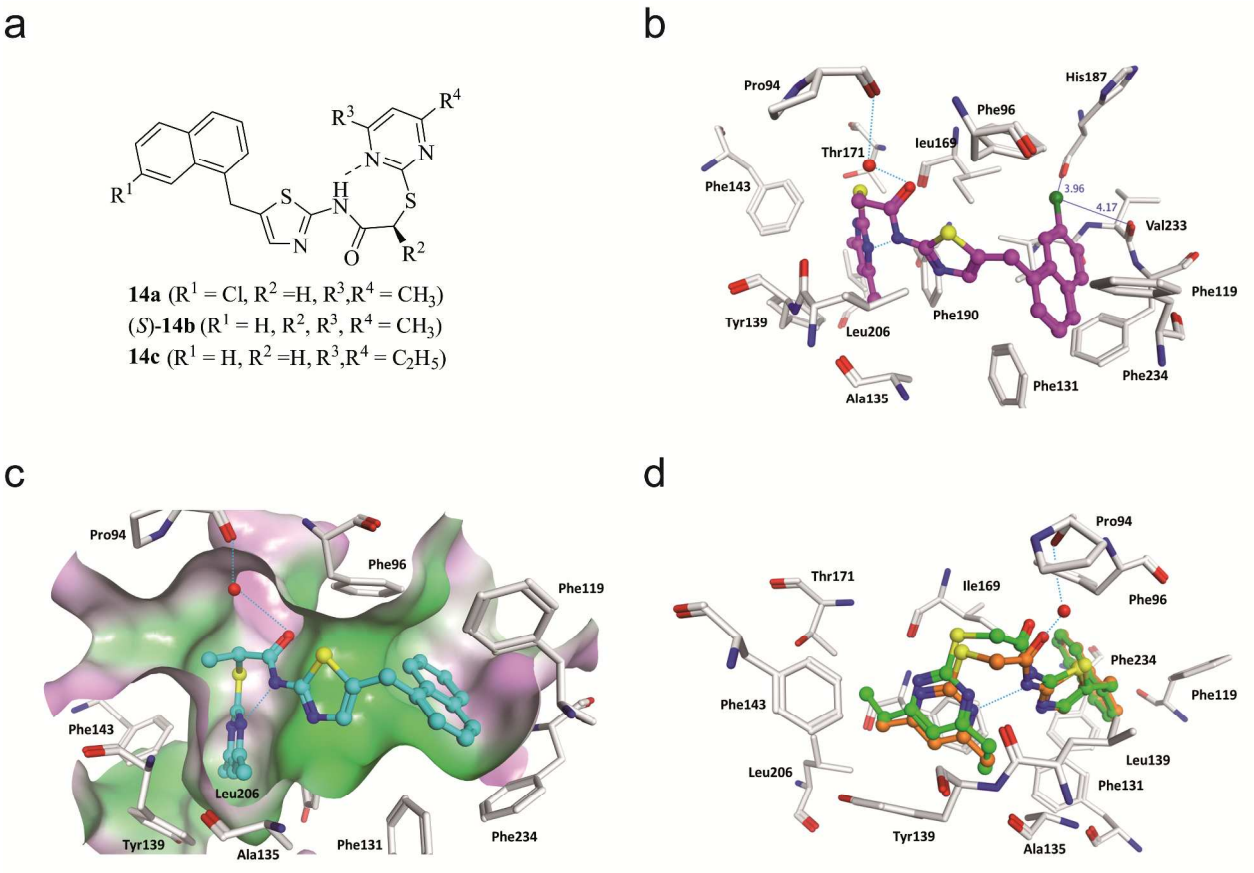

Figure 2. Docking poses derived for the envisaged SirReals **14a-c**. (a) Chemical structures used for docking studies. (b) Docking pose derived for **14a** (colored magenta). Distances between the halogen atom and the two carbonyl groups of His187 and Val233 are shown as blue lines with distances given in Angstrom. (c) Docking pose derived for (*S*)-**14b** (colored cyan). The methyl group ((*S*)-configuration) is orientated towards the exit of the 'selectivity pocket' which can accommodate longer alkyl groups. The molecular surface of the binding pocket is displayed and colored according to the hydrophobicity (green=hydrophobic, magenta= hydrophilic). (d) Docking pose derived for **14c** (colored green) in comparison with the X-ray structure of **10**

(colored orange). The larger ethyl groups of the pyrimidine ring cause steric clashes with Ala135 and Leu206 and, as a consequence, the H-bond to the conserved water molecules is lost. Hydrogen bonds are shown as dashed cyan colored lines, water molecules as red spheres.

To establish a well-defined SAR model, we set up a synthesis platform to generate a 2-aminothiazole library that was directed to yield compounds with a broad structural variety, particularly in the arylmethyl and pyrimidine parts of the ligand (Scheme 2).

Scheme 2. Synthesis platform utilized to generate the 2-aminothiazole library[a]

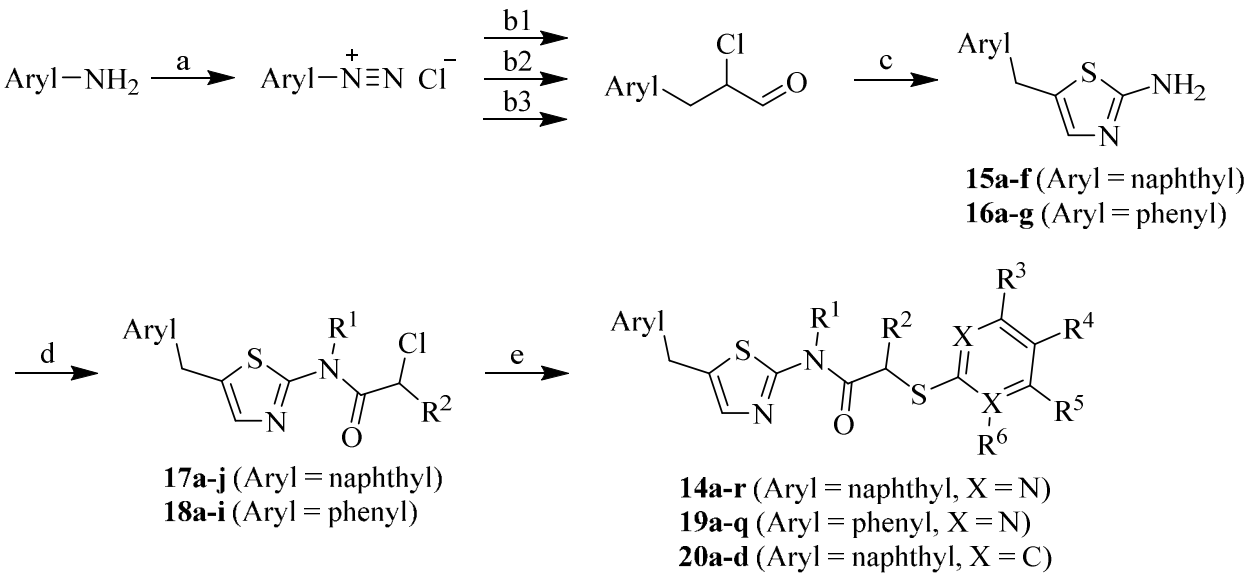

[a]Reagents and conditions: (a) $NaNO_2$, HCl, water, -5 – 0 °C, 10 min; (b1) acrolein, $CuCl_2$ x 2 H_2O, acetone, 3 h; (b2) $NaHCO_3$, MgO; then acrolein, $CuCl_2$ x 2 H_2O, acetone, 3 h; (b3) $FeCl_3$ x 6 H_2O, HCl, water, -5 – 0 °C; then $CuCl_2$ x 2 H_2O, HCl, acetone/ethanol, -5 – 0 °C; then acrolein, acetone/water, 4h; (c) thiourea or N-methylthiourea, ethanol, reflux, 2 h; (d) acyl chloride, DIPEA, acetonitrile, 0 °C to rt, 2 h; (e) aromatic thiol, Na_2CO_3, KI, DMSO, 2 h.

The biggest challenge within the synthesis of the SirReals was the preparation of α-chloropropanals *via* Meerwein reaction,[33] due to the instability of some arenediazonium salts,

especially the naphthalenediazonium salts.[34] In order to overcome these issues, we had to use three different methods to obtain sufficient amounts of the appropriate α-chloropropanals.[35] Toluene- and methoxybenzenediazonium salts could only be converted into the appropriate α-chloropropanals under standard Meerwein conditions in a neutral medium,[35a] while halogenated benzenediazonium salts, as well as the diazonium salt from 4-phenylaniline, successfully reacted in an acidic medium. For the synthesis of the 5-(naphthylmethyl)thiazol-2-amine derivatives **15a-f**, we followed a modified version of the Meerwein reaction published by Obushak et al.[35b] Initially, naphthalenediazonium chlorides were treated with iron(III) chloride in an aqueous solution to obtain the naphthalenediazonium tetrachloroferrates(III). An exchange reaction with $CuCl_2$ in acetone resulted in the precipitation of the naphthalenediazonium tetrachlorocuprates(II), which were isolated and used as a fine crystalline powder for the subsequent reaction with acrolein.[35b] With this protocol, we were able to generate the desired naphthyl derivatives **15b-c,** which could not be synthesized under standard Meerwein conditions, neither in an acidic nor in a neutral medium. For those naphthylamines that could be transformed into the corresponding α-chloropropanals using standard Meerwein conditions to a small extent,[35a] the modified version of the Meerwein reaction enabled us to increase the yield of this reaction largely. However, due to the time-consuming protocol of the modified Meerwein reaction, it was exclusively used to synthesize the naphthyl derivatives **15a-f** and compound **16g**, which could not be generated in satisfying yields applying standard Meerwein conditions. The α-chloropropanals were immediately converted into the aminothiazole scaffold (**15a-f**, **16a-g**) by condensation with thiourea.[35a] The aminothiazoles were subsequently chloroacetylated[32] to yield **17a-j** and **18a-i**, followed by a nucleophilic substitution with an aromatic thiol to generate compounds **14a-r**, **19a-q** and **20a-d**. The synthesis of the halogenated 1-naphthylamines (**21a-c**),

which were needed as starting materials for the synthesis of the halogenated inhibitors (**14a, 14d, 14f, 14g, 14i**), is illustrated in Scheme 3 by the example of the chlorinated 1-naphthylamines **21a-b**. Starting with the nitration of 2-aminonaphthalene-1-sulfonic acid followed by a desulfonation[36] the isomers of the respective nitronaphthalenamines **22a-b** were separated by flash chromatography. Halonitronaphthalenes **23a-c** were synthesized by applying Sandmeyer conditions.[37] Finally, the halogenated 1-naphthylamines **21a-c** were obtained by a reduction of the nitro group with $SnCl_2$.

Scheme 3. Synthesis of chlorinated 1-naphthylamines as starting material for further syntheses[a]

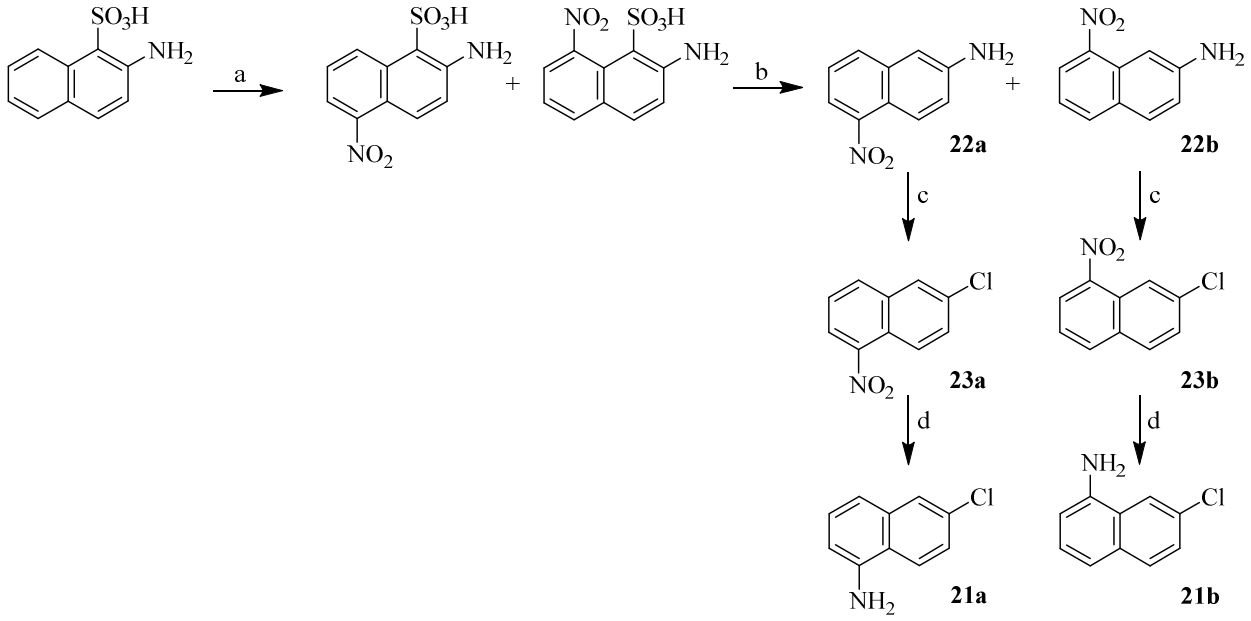

[a]Reagents and conditions: (a) H_2SO_4, KNO_3, -15 °C, 40 min; (b) H_2SO_4/water (1:1), reflux, 40 min; (c) glacial acid, H_2SO_4, $NaNO_2$, 15-20 °C, 15 min; then CuCl and HCl, rt, 1 - 4 h; (d) $SnCl_2$ x 2 H_2O, ethanol, rt, 4 – 24 h.

The synthesized SirReal derivatives were evaluated for their inhibitory activity against hSirt1 and hSirt2 in a biochemical *in vitro* assay that was previously described.[38] The *in vitro* inhibition

data of the aminothiadiazoles (**13a-h**) and the aminothiazole derivatives **20a-d**, **24a-b**, **25**, **26a-b** and **27-32**, which strongly deviate from the original scaffold is summarized in Table 1. Aminothiazoles (**9-10**, **14a-r**, **19a-q**) and their *in vitro* inhibition of hSirt1 and hSirt2 are shown in Table 2.

Table 1. *In vitro* inhibition of hSirt1 and hSirt2 by aminothiadiazoles **13a-h** and aminothiazoles **20a-d**, **24a-b**, **25**, **26a-b** and **27-32**

Shared scaffold or complete chemical structure	compd	R^1	R^2	hSirt1 inhibition %@conc. [µM] or IC_{50} ± SE [µM]	hSirt2 inhibition %@conc. [µM] or IC_{50} ± SE [µM]
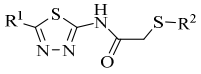	**13a**	1-naphthylmethyl	4,6-dimethylpyrimidin-2-yl	n.i.@ 200 µM[c]	1.89 ± 1.50
	13b	phenyl	5,6-diphenyl-1,2,4-triazin-3-yl	n.i.@ 200 µM	19.9 ± 31.7
	13c	4-chlorobenzyl	4,6-dimethylpyrimidin-2-yl	n.i.@ 200 µM	30.9 ± 20.5
	13d	4-bromobenzyl	4,6-dimethylpyrimidin-2-yl	n.i.@ 200 µM	167.7 ± 30.29
	13e	trifluoromethyl	4,6-dimethylpyrimidin-2-yl	12% @ 200 µM	502.8 ± 43.95
	13f	phenyl	4,6-dimethylpyrimidin-2-yl	n.i.@ 200 µM	19.9% @ 50 µM
	13g	benzyl	4,6-dimethylpyrimidin-2-yl	n.i.@ 200 µM	17.8% @ 50 µM
	13h	methyl	4,6-dimethylpyrimidin-2-yl	n.i.@ 200 µM	n.i. @ 50 µM
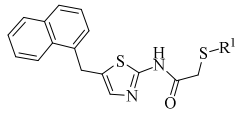	**20a**	3-hydroxyphenyl		n.i.@ 200 µM	143 ± 27.4
	20b[a]	3,5-dimethylphenyl		16% @ 200 µM	207 ± 27.4
	20c	2-aminophenyl		n.i.@ 200 µM	36% @ 50 µM
	20d	4-chlorophenyl		n.i.@ 200 µM	n.i. @ 50 µM
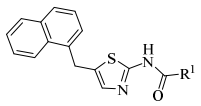	**24a**	CH_3		n.i.@ 200 µM	84% @ 500 µM n.i. @ 50 µM
	24b	C_5H_{11}		n.i.@ 200 µM	77% @ 500 µM 48% @50 µM n.i. @ 10 µM
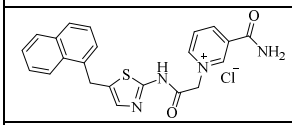	**25**			39% @ 200 µM	289 ± 127
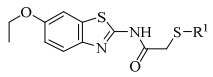	**26a**	4,6-dimethylpyrimidin-2-yl		16% @ 200 µM	77.8 ± 7.62
	26b[b]	4-hydroxy-6-propyl-pyrimidin-2-yl		n.i.@ 200 µM	n.i. @ 50 µM
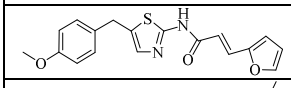	**27**			28% @ 200 µM	18% @ 50 µM
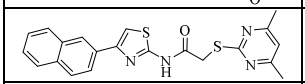	**28**			23% @ 200 µM	35% @ 50 µM
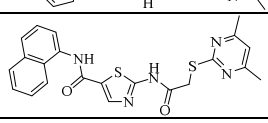	**29**			n.i.@ 200 µM	33.0 ± 15.4

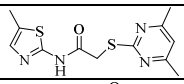	**30**			n.i.@ 200 µM	24% @ 250 µM
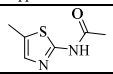	**31**			n.i.@ 200 µM	n.i. @ 50 µM
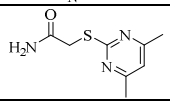	**32**			n.i.@ 200 µM	n.i. @ 50 µM

[a]Compound previously published by our group[30]

[b]Sirtuin inhibitor presented by Kazantsev et al.[39]

[c]n.i.: inhibition @ conc. [µM] < 10%

Among the aminothiadiazoles, compound **13a**, bearing a 1-naphthylmethyl and a 4,6,-dimethylpyrimidine moiety, displays the most potent hSirt2 inhibition. This is consistent with the previously published SirReal-mediated inhibition of hSirt2.[30] However, a switch from the aminothiazole to the aminothiadiazole scaffold was shown to lead to a loss in potency, and was therefore not further investigated. Furthermore, we observed a substantial decrease in potency for those compounds that strongly deviate from the original scaffold (**20a-d**, **24a-b**, **25**, **26a-b** and **27-32**, Table 1). Thus, we hypothesize that the unique mechanism of SirReal-mediated hSirt2 inhibition is restricted to compounds that display a high extent of similarity to the parent compounds **9** or **10**. By disassembling our lead structure **10** into fragments (**24a**, **30-32**, Table 1), we clearly demonstrate that the presence of all three functional elements, namely: arylmethyl, aminothiazole, and 4,6-dimethylpyrimidine is crucial for efficient inhibition of hSirt2 activity.

Table 2. *In vitro* inhibition of hSirt1 and hSirt2 by aminothiazoles **9-10**, **14a-r**, **19a-q**

Shared scaffold:

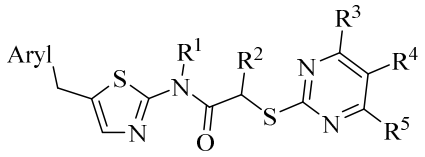

compd	Aryl	R1	R2	R3	R4	R5	hSirt1 inhibition %@conc. [μM] or IC_{50} ± SE [μM]	hSirt2 inhibition %@conc. [μM] or IC_{50} ± SE [μM]
9[a]	phenyl	H	H	CH_3	H	CH_3	15% @ 200 μM	3.75 ± 0.83
10[a]	naphthalen-1-yl	H	H	CH_3	H	CH_3	n.i.@ 200 μM	0.44 ± 0.08
14a	7-chloronaphthalen-1-yl	H	H	CH_3	H	CH_3	29% @ 200 μM	0.18 ± 0.02
rac-**14b**	naphthalen-1-yl	H	CH_3	CH_3	H	CH_3	17% @ 200 μM	0.42 ± 0.04
(*S*)-**14b**	naphthalen-1-yl	H	(*S*)-CH_3	CH_3	H	CH_3	n.i.@ 200 μM	0.26 ± 0.03
(*R*)-**14b**	naphthalen-1-yl	H	(*R*)-CH_3	CH_3	H	CH_3	n.i.@ 200 μM	9.77± 4.78
14c	naphthalen-1-yl	H	H	C_2H_5	H	C_2H_5	n.i.@ 200 μM	45.6 ± 24.6
14d	7-bromonaphthalen-1-yl	H	H	CH_3	H	CH_3	n.i.@ 200 μM[b]	0.21 ± 0.02
14e	2-methylnaphthalen-1-yl	H	H	CH_3	H	CH_3	n.i.@ 200 μM	0.31 ± 0.01
rac-**14f**	7-chloronaphthalen-1-yl	H	C_2H_5	CH_3	H	CH_3	n.i.@ 200 μM	0.32 ± 0.05
14g	6-chloronaphthalen-1-yl	H	H	CH_3	H	CH_3	20% @ 200 μM	0.48 ± 0.05
rac-**14h**	naphthalen-1-yl	H	C_2H_5	CH_3	H	CH_3	35% @ 200 μM	0.54 ± 0.06
rac-**14i**	7-chloronaphthalen-1-yl	H	CH_3	CH_3	H	CH_3	n.i.@ 200 μM	0.54 ± 0.08
14j	naphthalen-1-yl	H	H	CH_3	H	H	n.i.@ 200 μM	1.45± 0.18
rac-**14k**	naphthalen-1-yl	H	CH_3	H	H	H	21% @ 200 μM	1.92 ± 0.42
14l[a]	naphthalen-1-yl	H	H	H	H	H	17% @ 200 μM	2.34 ± 0.42
14m	naphthalen-1-yl	H	H	CH_3	CH_3	CH_3	n.i.@ 200 μM	15.0 ± 2.11
14n	naphthalen-2-yl	H	H	CH_3	H	CH_3	n.i.@ 200 μM	65.0 ± 31.7
14o	naphthalen-1-yl	H	H	OH	H	C_3H_7	22% @ 200 μM	127.2± 13.4
14p[a]	naphthalen-1-yl	CH_3	H	CH_3	H	CH_3	n.i.@ 200 μM	>100
14q	naphthalen-1-yl	H	H	OH	H	CH_3	n.i.@ 200 μM	35% @ 50 μM
14r	naphthalen-1-yl	H	H	NH_2	H	NH_2	n.i.@ 200 μM	25% @ 50 μM
19a	3-ethoxyphenyl	H	H	CH_3	H	CH_3	n.i.@ 200 μM	1.33 ± 0.15
19b	3-methylphenyl	H	H	CH_3	H	CH_3	18% @ 200 μM	1.64 ± 0.40
19c	4-chlorophenyl	H	H	CH_3	H	CH_3	n.i.@ 200 μM	3.40 ± 0.49
19d	4-methylphenyl	H	H	CH_3	H	CH_3	16% @ 200 μM	4.72 ± 5.55
rac-**19e**	4-methoxyphenyl	H	CH_3	CH_3	H	CH_3	27% @ 200 μM	14.6 ± 9.24
19f[a]	phenyl	H	H	H	H	H	12% @ 200 μM	16.8 ± 4.96
rac-**19g**	4-biphenyl	H	CH_3	CH_3	H	CH_3	14% @ 200 μM	33.0 ± 13.8
19h	4-biphenyl	H	H	CH_3	H	CH_3	29% @ 200 μM	164.5 ± 23.4
19i	4-biphenyl	H	H	C_2H_5	H	C_2H_5	10% @ 200 μM	31% @ 50 μM
19j	2-methylphenyl	H	H	CH_3	H	CH_3	14% @ 200 μM	52% @ 50 μM
19k	4-methoxyphenyl	H	H	CH_3	H	CH_3	n.i.@ 200 μM	48% @ 50 μM
19l	4-methoxyphenyl	H	H	C_2H_5	H	C_2H_5	17% @ 200 μM	48% @ 50 μM
19m	4-chlorophenyl	H	H	C_6H_5	H	C_6H_5	11% @ 200 μM	46% @ 50 μM
rac-**19n**	4-methoxyphenyl	H	CH_3	C_2H_5	H	C_2H_5	18% @ 200 μM	40% @ 50 μM
19o	4-chlorophenyl	H	H	C_2H_5	H	C_2H_5	18% @ 200 μM	38% @ 50 μM
19p	2-methylphenyl	H	H	H	H	H	11% @ 200 μM	n.i. @ 50 μM
19q	3-methylphenyl	H	H	C_2H_5	H	C_2H_5	n.i.@ 200 μM	n.i. @ 50 μM

[a]Compounds previously published by our group[30]

[b]n.i.: inhibition @ conc. [μM] < 10%

Analyzing the data of Table 2, we can confirm the findings of our preliminary SAR model,[30] highlighting the importance of the 4,6-dimethylpyrimidine moiety for the binding of the ligand to

the newly formed 'selectivity pocket'. On the one hand, we show that ligands lose their affinity without the methyl groups at the pyrimidine ring in position 4 and/or 6 (**14j-l**), on the other hand we reveal that a higher degree of methylation (**14m**) or bulkier substituents (**14c**, **19l**, **19n-o**) cause a decrease in potency, as predicted by molecular docking studies (Figure 2d). Furthermore, we could show that polar substituents at the pyrimidine ring, e.g. -OH or -NH_2 (**14q-r**), are not beneficial in terms of potency. The inhibition data of the novel ligands with 2-naphthyl (**14n**), biphenyl (**19g-i**) or substituted phenyl moieties (**19a-e**, **19j-q**), which were generated to study the impact of structural changes of the arylmethyl moiety, clearly indicates the superiority of the 1-naphthyl substituted SirReals. We were able to rationalize the observed loss of *in vitro* potency caused by replacing the 1-naphthyl moiety with other aryl substituents e.g. biphenyl, by means of docking studies. These indicate a steric clash with the residues Val233, Phe234 and Phe235 of the binding pocket (data not shown). Comparing the substituted phenyl ligands with their parent compound **9**, we conclude that a substitution in position 3 is beneficial in terms of hSirt2 inhibition (**19a-b**), whereas other substitution patterns lead to a decrease in potency (e.g. **19c-d**, **19j**). This observation is reflected by the docking results (Table S1) where we propose that the 4-position of the phenyl ring is unfavorable for substitution due to the close proximity of Phe234, whereas in the 3-position the substituent protrudes into the acyl-lysine channel (not shown). As predicted by molecular docking, an alkylation in the α-position of the amide leads to increased potency of the (*S*)-enantiomer in the case of the methyl group (**(*S*)-14b**). Compared to *rac*-**14b**, an ethyl group already led to a decrease in potency (*rac*-**14h)**. As the ethyl compounds (*rac*-**14h**, *rac*-**14f**) additionally turned out to be poorly soluble, we therefore did not separate the enantiomers of those compounds. Most importantly, however, we improved the *in vitro* activity of our lead structure by a chlorination or bromination of the naphthyl residue in position 7 (**14a**,

14d). We were able to rationalize these results by binding free energy studies in combination with molecular docking (See Methods section for further details). Using docking poses calculated with the program GLIDE (Schrödinger LLC, New York, USA) and subsequent refinement using the program AMBER and a GBSA solvation model implemented in MOE 2012.10 (Chemical Computing Group, Montreal, Canada) we observed a correlation between the experimental pIC_{50} values and the calculated binding energies E_{GBSA} (r^2=0.67, RMSE 0.60, q^2_{LOO}=0.62, Figure S1). An improvement of the model was derived by including two topological descriptors describing the ligand structures ("diameter" and surface descriptor "PEOE_VSA4", see Methods section). The resulting model showed the following equation:

pIC_{50} = -1.474 – 0.192 "diameter" – 0.032 "PEOE_VSA4" – 0.195 "E_{GBSA}"

"Diameter" is the largest value in the distance matrix dimension of the molecules and is an indicator of the dimension of the molecules. Increasing the "diameter" of the inhibitors is unfavorable as well as increasing the surface descriptor "PEOE_VSA4". The final quantitative structure activity relationship (QSAR) model is able to rationalize the observed *in vitro* activities of the developed inhibitors (r^2=0.81, RMSE 0.45, q^2_{LOO}=0.76, Figure S2). The QSAR model was further tested by 10-fold cross validation using randomly selected 20% of the compounds as test set. The calculated $q^2_{L20\%O}$ value of 0.74 supports the robustness of the model.

Moreover, we were able to rationalize these results with a crystal structure of hSirt2 in complex with **14d** and NAD^+ (Figure 3).

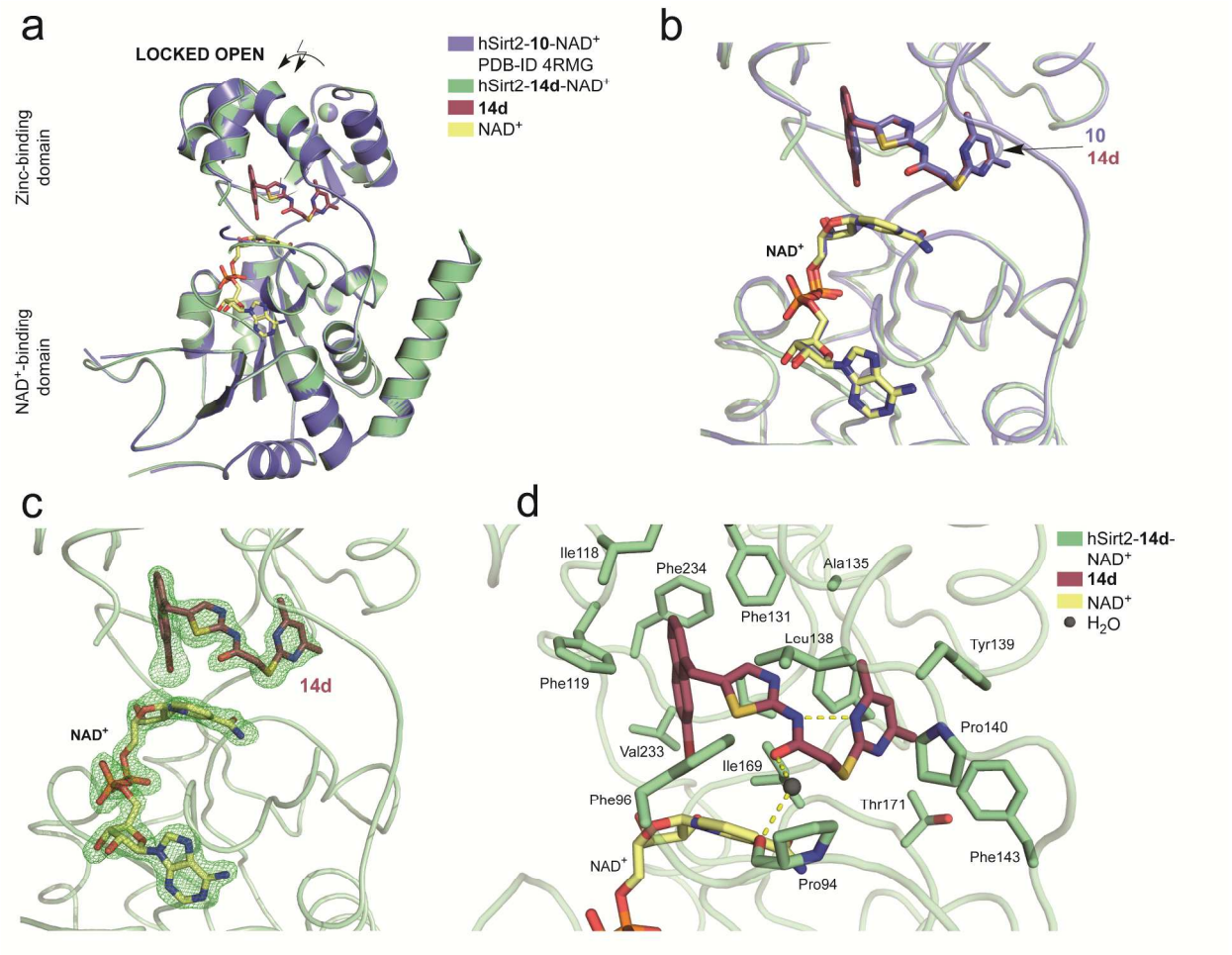

Figure 3. 14d of the hSirt2-**14d**-NAD$^+$ complex binds to hSirt2 in a similar fashion as observed for **10** of the hSirt2-**10**-NAD$^+$ complex. (a) Superposition of the hSirt2-**10**-NAD$^+$ complex (cartoon: slate blue, PDB-ID 4RMG) with the crystal structure of hSirt2-**14d**-NAD$^+$ (cartoon: pale green; **14d**: raspberry sticks; NAD$^+$: pale yellow sticks). Both complexes adopt the 'locked open'-conformation (RMSD of all Cα-atoms: 0.33 Å). (b) **14d** and NAD$^+$ of the hSirt2-**14d**-NAD$^+$ complex assume a very similar position within the active site of hSirt2 as **10** and NAD$^+$ of the hSirt2-**10**-NAD$^+$ structure. (c) **14d** as well as NAD$^+$ are well-defined by the electron density. σ-weighted iterative OMIT maps are shown as green mesh and contoured at 3.0σ. (d) Interactions of **14d** with hSirt2. Interacting residues are represented as sticks (green). Phe190,

Ile232 are not labeled and Leu206 is not shown for the sake of clarity. The water molecule is represented as a black sphere and hydrogen bonds as dashes yellow lines.

The crystal structure reveals that **14d,** as well as NAD^+, assume a very similar position within the active site of hSirt2 compared to **10** and NAD^+ of the hSirt2-**10**-NAD^+ structure (Figure 3a-b). We were not able to observe a σ-hole interaction in our co-crystal structure as suggested by the docking study. Binding of **14d** is mainly driven by hydrophobic interactions with the side chains of the residues forming the extended C-site (ECS), the acyl-lysine binding site as well as the 'selectivity pocket' at the hinge region. The 7-bromonaphthyl substituent fills the lipophilic naphthyl binding site more efficiently than the unsubstituted naphthyl moiety, and thereby allows further hydrophobic interactions. The carbonyl-O of the amide also forms a water-mediated hydrogen bond to the backbone carbonyl-O of Pro94. As it was already observed in the crystal structure of hSirt2-**10**-NAD^+, **14d** also forms an intramolecular hydrogen bond between the amide N-H and one of the nitrogen atoms of the dimethylpyrimidine ring. (Figure 3d). To see, whether the combination of beneficial substitution patterns would lead to a further increase in potency, we combined a 7-chloro substituent with an α-methylation in the amide part. Yet, we did not detect an additive effect by combining a 7-halonaphthyl moiety with a methylation in the α-position of the amide (*rac*-**14i)**.

To assess the cellular activity of the 7-halonaphthyl derivatives, we utilized immunofluorescence microscopy and western blot experiments, showing an enhanced tubulin hyperacetylation for **14a**, when compared to DMSO control (Figure 4, for raw images see Figure S3, for western blots Figure S4).

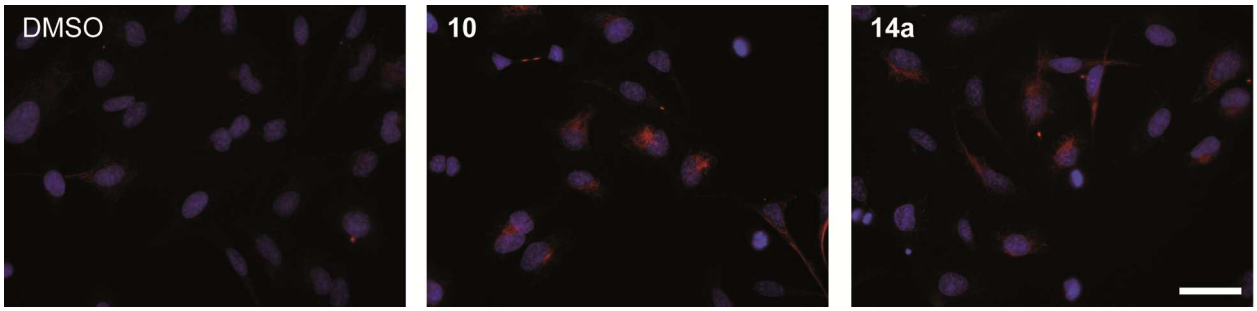

Figure 4. Optimized aminothiazole **14a** induces tubulin hyperacetylation in cultured HeLa cells. Acetylation level of the microtubule network (red) in the presence or absence of sirtuin inhibitors (10 μM). Treatment of HeLa cells with **14a** leads to higher acetylation levels of the microtubule network as compared to the DMSO treated cells (negative control). **10** was used as a positive control. Nuclei were DAPI-stained (blue). The scale bar represents 10 μm.

Treatment with the optimized SirReal derivative **14a** leads to hyperacetylation of the microtubule network in a similar manner as observed for **10,** which was used as a positive control. While compounds **14a** and **10** both lead to a significant increase in tubulin hyperacetylation at a concentration of 20 μM, **14a** also induces a significant gain in tubulin acetylation at only 10 μM (Figure S4). Thus, we could show that the improved *in vitro* potency of **14a** is also relevant under physiological conditions. Of note, the halogenated derivatives were badly soluble in cell culture media and may therefore be limited in their efficacy at higher concentrations.

DISCUSSION AND CONCLUSION: Starting out from compounds **9** and **10** as potent and selective hSirt2 inhibitors, we established a synthesis platform to systematically probe the limits of modification within this scaffold. We were able to elaborate a well-defined SAR model for both, the arylmethyl and the pyrimidine moiety. Guided by the structural knowledge, revealed by hSirt2-**9**/**10** co-crystals as well as molecular docking studies, we were able to improve the *in vitro* hSirt2 inhibition of both lead structures, **9** and **10**. Moreover, the cellular activity of the improved aminothiazole inhibitor **14a** was validated by tubulin hyperacetylation in HeLa cells. In combination with the herein reported co-crystal structure, our SAR model will be the foundation for further developments of the Sirtuin Rearranging Ligands as valuable biological tool compounds to gain deeper insight into sirtuin biology and to probe the druggability of sirtuins.

EXPERIMENTAL SECTION:

1. Protein expression and purification: $hSirt1_{133-747}$ was expressed as a GST-tagged enzyme and purified as described previously.[40] $hSirt2_{25-389}$ was expressed N-terminally tagged with His_6[41] with minor modifications.[40] $hSirt2_{56-356}$ was expressed and purified according to Rumpf et al.[30]

2. *In Vitro* Testing: Potency of hSirt1 and hSirt2 inhibition was determined with a fluorescence-based homogeneous assay using the substrate ZMAL (Cbz-Lys(acetyl)-AMC).[38] $hSirt1_{133-747}$ or $hSirt2_{25-389}$ were mixed with assay buffer (50 mM Tris, 137 mM NaCl, 2.7 mM KCl, pH 8.0), NAD^+ (final assay concentration 500 µM), the substrate ZMAL (final assay concentration 10,5 µM), the inhibitor dissolved in DMSO at different concentrations, or DMSO only as a control (final DMSO concentration 5% (v/v)). To ensure initial state conditions, total substrate conversion of controls was adjusted to approximately 15% - 30%. The assay was performed in 96-well plates with a reaction volume of 60 µL per well. All determinations were performed at least in duplicates. After an incubation of 4 h at 37 °C and 140 rpm, deacetylation reaction was stopped by the addition of 60 µL of a stop solution containing trypsin and nicotinamide (50 mM Tris, 100 mM NaCl, 6.7% (v/v) DMSO, trypsin 5.5 U μL^{-1}, 8 mM nicotinamide, pH 8.0). The reaction mixture was further incubated for 20 min at 37 °C and 140 rpm. Fluorescence intensity was measured in a microplate reader (BMG Polarstar, λ_{ex} = 390 nm, λ_{em} = 460 nm). Rates of inhibition were determined by using the controls, containing no inhibitor, as a reference. Graphpad Prism software (La Jolla, CA) was employed to determine IC_{50} values.

3. Data collection, structure solution and refinement: Data were collected at 100 K at X06SA beamline of the Swiss Light Source (Villigen, Switzerland) equipped with a Pilatus 6M detector at a wavelength of 1.0 Å with oscillations of 0.5°. Data were processed with XDS[42] and scaled based on the CC1/2 criterion[43] using Aimless.[44] Data collection statistics are shown in Table 5.

The structure was solved by molecular replacement with MOLREP[45] using the hSirt2-**10**-NAD^+-complex (PDB-ID 4RMG)[30] as a search model. The structural model was built in Coot[46] and refined with REFMAC.[47] **14d** was generated with the Grade Web Server (Global Phasing Ltd., United Kingdom) and placed into $2F_o$-F_c electron density maps using AFITT-CL (Version 2.1.0, OpenEye Scientific Software, Inc., Santa Fe, NM, USA.). All residues except Pro99, Ser100 and Thr101 were included in the model. The N-terminal glycine, histidine and methionine originate from the TEV cleavage site and the *NdeI*-restriction site of the modified pET15b- expression vector. The structure was validated using the Molprobity server[48] and PROCHECK.[49] σ-weighted iterative OMIT maps were generated with Phenix.[50] RMSD values were determined with SUPERPOSE[51] and images were prepared with Pymol (The Pymol Molecular Graphics System, Version 1.7, Schrödinger, LLC).

Table 5. Data collection and refinement statistics

	hSirt2-14d-NAD^+
Data processing	
PDB accession #	5DY4
Spacegroup	*I*2
a, b, c (Å)	84.30, 55.43, 96.18
α, β, γ (°)	90, 114.91, 90
Resolution (Å)	46.78–1.77 (1.81–1.77)
Unique observations	38622 (2201)
Observations	260647 (15296)
Completeness (%)	98.2 (98.1)
Multiplicity	6.7 (6.9)
R_{merge} [1]	0.095 (2.050)
$I / \sigma I$	10.3 (1.0)
CC1/2	0.998 (0.554)

Refinement	
Resolution (Å)	46.78–1.77 (1.81–1.77)
No. Amino acids	300
No. Atoms	2649
Protein	2391
14d	30
NAD^+	44
Waters	183
Zn^{2+}	1
R_{cryst}/R_{free} (%) [2]	17.5/21.3
***B* factors (Å^2)**	
Protein	33.71
14d	27.88
NAD^+	29.05
Waters	38.64
Zn^{2+}	27.58
RMSD bond length (Å)	0.013
RMSD angles (°)	1.65
Ramachandran plot statistics	
Most favoured region (%)	93.2
Additional allowed region (%)	6.5
Generously allowed region (%)	0.3
Disallowed region (%)	0.0

Values in parentheses represent the highest resolution shell.

[1] $R_{merge} = \sum_{hkl} [(\sum_i |I_i - \langle I \rangle|) / \sum_i I_i]$

[2] $R_{cryst} = \sum_{hkl} ||F_{obs}| - |F_{calc}|| / \sum_{hkl} |F_{obs}|$

R_{free} is the cross-validation R factor computed for a test set of 5 % of unique reflections selected randomly.[52] Ramachandran statistics as defined by PROCHECK.[49]

4. Protein crystallization: Crystallization assays were set up with the Oryx Nano pipetting robot (Douglas Instruments, United Kingdom) using the vapor diffusion sitting drop method (Intelli-Plate 96-3 Low Profile, Art Robbins Instruments, USA) at 4 °C. Prior to crystallization, hSirt2$_{56-}$

$_{356}$ (20 mg mL^{-1}) was incubated with **14d** (100 mM stock solution in DMSO, 1% (v/v) final DMSO concentration) and NAD^+ (100 mM stock solution in 25 mM Tris/HCl, 150 mM NaCl, pH 8.0, final concentration 10 mM, Sigma-Aldrich, Germany). Crystals of the hSirt2-**14d**-complex were obtained after 2 days in a solution containing 27% (w/v) PEG 3350 in 0.05 M HEPES buffer at pH 7.0 with a protein solution to reservoir ratio of 3:1. The crystal was mounted on a nylon loop and cryoprotected by the addition of 20% (v/v) glycerol.

5. Cell Culture: HeLa (ATCC-2) cells were cultured in Dulbecco's Modified Eagle's Medium (high glucose) supplemented with 10% (v/v) fetal calf serum, 100 µg/ml kanamycin (all reagents from Sigma-Aldrich) in a humidified incubator at 37 °C with 5% CO_2. For microscopic analysis, 0.5 x 10^4 cells were seeded on 12 mm diameter coverslips placed in 24-well plates and incubated overnight before the experiment. For immunoblotting, 1.5 x 10^4 cells were seeded per well of 24-well plates and incubated overnight. The drugs were added to cells for 1 hour from 10 mM stock solutions in DMSO. Controls contained the corresponding amount of vehicle (DMSO).

6. Immunoblotting: For the detection of acetylated tubulin, total tubulin and glyceraldehyde-3-phosphate dehydrogenase (GAPDH) levels in cellular samples, we kept the cells at 37 °C and washed them with prewarmed PBS. Next, the cells were lysed in 100 µL 1x reducing sample buffer containing protein inhibitor mix and 2 mM EDTA (Sigma-Aldrich). Samples were centrifuged at 10,000 g at 4°C for 5 min and the supernatants were stored at -70 °C. Samples were analyzed by SDS-PAGE and blotted onto polyvinylidene difluoride membrane (Millipore). The blot was developed sequentially using a monoclonal mouse antibody against acetylated alpha-tubulin at Lys-40 (1:5000, clone 6-11B-1), than using a monoclonal mouse antibody against alpha-tubulin (1:5000, clone DM1A), next using a monoclonal mouse antibody against GAPDH (1 µg/mL, CB1001, clone 6C5, Calbiochem). Antibodies were detected by anti-mouse

IgG-peroxidase conjugate (Fc-specific), (1:5000, Sigma-Aldrich). Peroxidase reaction detected using Immobilon Western substrate (Millipore) by a Bio-Rad ChemiDoc MP Imaging system and its ImageLab 4.1 software. Intensity of spots was analysed by ImageJ 1.49 using Measure command and subtracting background values. The sample values were normalized by the average control value on the corresponding blot.

7. Immunofluorescence microscopy: Immunofluorescence microscopy was performed as previously reported.[30]

8. Computational Methods: 3D structures of all compounds in this study were generated from SMILES strings, and a subsequent energy minimization was carried out using the MMFF94x force field implemented in Molecular Operating Environment System (MOE) 2012.10 (Chemical Computing Group, Montreal, Canada). All compounds were used in the protonation state at physiological level. A maximum of 100 conformations were generated for each ligand using the Conformational Search module implemented in MOE. All protein structures were prepared by using the Structure Preparation module in MOE. Hydrogen atoms were added and the protonation state for titratable amino acids was calculated using the Protonate 3D module in MOE. Protein structures were energy minimized using the AMBER99 force field[53] with a tethering force constant of (3/2) kT / 2 (σ = 0.5 Å) for all atoms during the minimization. AM1-BCC charges were used for ligands.[54] All molecules except the zinc ion were removed from the structures. Protein-ligand docking was performed using program GLIDE (Suite 2012-5.8, Schrödinger LLC, New York, USA). The position of the inhibitor **10** in its crystal structure with hSirt2/Ac-Lys-H3 peptide (PDB ID 4RMH) was used to define the size of the grid box (10 Å radius). Docking was performed using GLIDE-Extra Precision (XP). The ligand was treated as flexible and 20 docking poses were calculated for each inhibitor. All other options were left at

their default values. The top-ranked pose from each docking run was included in the final analysis and viewed graphically together with the protein structure using the program MOE 2010.13 (Chemical Computing Group, Montreal, Canada). Using the docking setup, **10** could be correctly docked into its crystal structure with RMSD values below 0.5 Å (PDB ID 4RMG and 4RMH).[30] Also, other active aminothiazole derivatives were predicted to adopt a similar binding mode as was observed for **10**. Binding free energies for the inhibitors in this study were calculated using the top-ranked docking poses. Structurally conserved water molecules included for docking studies were maintained during the geometry optimization of the complexes. The protein-inhibitor complexes were energy minimized using the AMBER PFROSST force field and the GBSA solvation model implemented in MOE 2012.10. Using the resulting ΔE_{GBSA} value as descriptor, a significant correlation to the pIC_{50} values was observed (r^2=0.67, RMSE=0.60) for the 30 compounds for which an IC_{50} and exact stereochemistry was determined (Figure S1). Besides the correlation coefficient r^2, the model was also tested using leave one out (LOO) cross-validation (q^2_{LOO}=0.62). Furthermore, we investigated the effect of other descriptors like ligand charge, diameter, or polar surface descriptors for establishing a QSAR model. We successfully applied this approach recently for establishing predictive models with high robustness.[55] Among 192 tested 2D descriptors in MOE, the "diameter" and the topological surface descriptor "PEOE_VSA+4" showed the highest correlation. A QSAR model based on three descriptors, namely "ΔE_{GBSA} score", "diameter", and "PEO_VSA+4" using MOE PLS methodology was generated and validated. The final PLS model yielded a correlation coefficient of r^2=0.81 (RMSE=0.45) and a q^2_{LOO} of 0.76 demonstrating the robustness of the model (Figure S2, Table S1). Since LOO cross-validation is sometimes misleading and resulting in too optimistic models, a more demanding cross-validation procedure was applied for the QSAR model. 10-fold cross

validation was carried out using randomly selected compounds (20%) as test set. Repeating this random splitting 10 times, resulted in a mean $q^2_{L20\%O}$ value of 0.74, demonstrating the robustness of the model. All results are summarized in Table S2 in the Supplementary Information.

9. Chemistry: Starting materials and reagents were obtained from commercial suppliers and used without further purification. Thin-layer chromatography (TLC) for reaction monitoring was performed with alumina plates coated with Merck silica gel 60 F_{254} (layer thickness: 0.2 mm) and analyzed under UV-light (254 nm). A mixture of ethyl acetate and cyclohexane (2:1) was used as mobile phase. If the purity of the synthesized compounds was not adequate, we performed flash column chromatography with TELOS Flash-LL Silica Columns 60M (0.040-0.063 mm, 230-400 mesh) as a stationary phase on a Biotage Isolera One automated flash purification system with UV-Vis detector. Cyclohexane and ethyl acetate was used as mobile phase and gradient was adjusted based on TLC results. Yields were not optimized. ^{1}H-NMR and ^{13}C-NMR spectra were recorded on Bruker Avance III HD spectrometer at 400 MHz and 100 MHz. The spectra are referenced against the NMR solvents and are reported as follows: ^{1}H: chemical shift δ (ppm), multiplicity (s = singlet, d = doublet, dd = doublet of doublets, t = triplet, q = quartet, quint = quintet, sex = sextet, m = multiplet, b = broad), integration, coupling constant (J in Hz). ^{13}C: chemical shift δ (ppm), abbreviations: (q) = quaternary carbons, quaternary carbons that could not be found in ^{13}C spectra but in HMBC or HSQC are additionally marked with an asterisk (*). The assignment resulted from HMBC and HSQC experiments. Purity was determined for all tested compounds by HPLC and UV detection (λ = 210 nm) and was > 95%. HPLC analysis was performed using the following conditions: Eluent A: H_2O containing 0.05% TFA, Eluent B: acetonitrile containing 0.05% TFA, Eluent C: n-

hexane, Eluent D: propan-2-ol, flow rate 1 mL min^{-1}. Method 1.1 (M1.1), analytical column, Phenomenex Synergi™ 4 μm MAX-RP 80 Å, 150 x 4.6 mm, isocratic conditions (A = 55%, B = 45%). Method 1.2 (M1.2), analytical column, Phenomenex Synergi™ 4 μm HYDRO-RP 80 Å, 250 x 4.6 mm. Method 1.3 (M1.3), analytical column, Phenomenex Synergi™ 4 μm POLAR-RP 80 Å, 150 x 4.6 mm. Method 2.1 (M2.1), analytical column, Phenomenex SynergiTM 4 μm MAX-RP 80 Å, 150 x 4.6 mm, isocratic conditions (A = 40%, B = 60%). Method 2.2 (M2.2), analytical column, Phenomenex Synergi™ 4 μm POLAR-RP 80 Å, 150 x 4.6 mm. Method 3 (M3), analytical column, Phenomenex Synergi™ 4 μm HYDRO-RP 80 Å, 250 x 4.6 mm, isocratic conditions (A = 30%, B = 70%). Method 4 (M4), analytical column, Phenomenex Synergi™ 4 μm HYDRO-RP 80 Å, 250 x 4.6 mm, isocratic conditions (A = 65%, B = 35%). Method 5 (M5), analytical column, Phenomenex Synergi™ 4 μm HYDRO-RP 80 Å, 250 x 4.6 mm, isocratic conditions (A = 5%, B = 95%). Method 6.1 (M6.1), analytical column, Phenomenex Synergi™ 4 μm HYDRO-RP 80 Å, 250 x 4.6 mm, linear gradient conditions (0−4 min, A = 90%, B = 10%; 4−29 min, linear increase to 100 % of B; 29−31 min, B = 100%; 31−40 min, A = 10%, B = 90%). Method 6.2 (M6.2), analytical column, Phenomenex SynergiTM 4 μm MAX-RP 80 Å, 150 x 4.6 mm. Method 6.3 (M6.3), analytical column, Phenomenex Synergi™ 4 μm HYDRO-RP 80 Å, 250 x 4.6 mm. Method 7 (M7), analytical column, Phenomenex Lux™ 5 μm CELLULOSE-1, 250 x 4.6 mm, linear gradient conditions (0−4 min, C = 90%, D = 10%; 4−30 min, linear increase to C = 50%, D = 50%; 30−36 min, linear gradient to C=90%, D=10%, 36–40 min C=90%, D=10%. Melting temperatures were determined in glass capillary tubes with the Stuart Melting Point Apparatus SMP2. Optical rotation was measured with a PerkinElmer Model 341 Polarimeter. Mass spectra with electrospray ionization (ESI) were recorded on an Advion expression CMS spectrometer, with electron ionization (EI) on an Agilent Technologies

6890 N Network GC-MS system. The synthesis of compounds **16e**,[35a] **22b**,[36] **23b**,[37] **33**,[56] has already been reported. Due to changes in the experimental procedure and to show unpublished characterization data, we have outlined the synthesis and the characterization data for those compound as well.

General Procedure for the Synthesis of 1,3,4-Thiadiazol-2-amines (**11a-e**):[31] A well-stirred mixture of thiosemicarbazide (1 equiv, 25 mmol), the carboxylic acid (1.2 equiv), and 8 mL of concentrated sulphuric acid was slowly heated to 80 – 90 °C and maintained at this temperature for 7 hours. After cooling, the reaction mixture was poured into ice water and was treated with concentrated ammonia to pH = 12. The crude product, which precipitated upon the addition of the ammonia, was filtered off and washed with water.

5-(1-Naphthylmethyl)-1,3,4-thiadiazol-2-amine (**11b**):[57] From thiosemicarbazide and 1-naphthylacetic acid. Yield: 3% of a beige solid. R_f: 0.15; ^{1}H-NMR (DMSO-D_6, δ [ppm]): 8.16-8.09 (m, 1H, naphthyl H-8), 7.98-7.92 (m, 1H, naphthyl H-5), 7.90-7.82 (m, 1H, naphthyl H-4), 7.60-7.43 (m, 4H, naphthyl H-2,3,6,7), 6.97 (bs, 2H, -NH_2), 4.62 (s, 2H, Ar-CH_2-Ar); ^{13}C-NMR (DMSO-D_6, δ [ppm]): 169.01 q (aminothiadiazole C-2), 158.20 q (aminothiadiazole C-5), 134.54 q (naphthyl C-1), 133.93 q (naphthyl C-4a), 131.66 q (naphthyl C-8a), 128.99 (naphthyl C-5), 128.18 (naphthyl C-4), 127.53 (naphthyl C-2), 126.74 (naphthyl C-7), 126.32 (naphthyl C-6), 126.11 (naphthyl C-3), 124.30 (naphthyl C-8), 33.80 (Ar-CH_2-Ar); ESI-MS(+): 242.1 $[M+H]^+$

General Procedure for Acylation of Thiazol-2-amines and 1,3,4-Thiadiazol-2-amines to generate amides (**12a-g**, **17a-j**, **18a-i**, **24a-b**, **31**, **37**, **43**, **44**):[32] To a solution of the amine (1 equiv, 2 mmol), dissolved in 10-30 mL acetonitrile, N,N-diisopropylethylamine (1.5 equiv) was added. The mixture was stirred and cooled to 0 °C. The acyl chloride (1.5 equiv) was

gradually added with stirring and cooling. After stirring for 2 h at room temperature, volatiles were evaporated. The red brown, oily residue was mixed with water (10-30 mL) and precipitates were collected by filtration. Precipitates were washed with water, hydrochloric acid (1 M), water, and dried to yield the corresponding amide.

2-Chloro-N-[5-[(7-chloro-1-naphthyl)methyl]thiazol-2-yl]acetamide (**17f**): From **15d** and 2-chloroacetyl chloride. Yield: 98% of a beige solid; R_f: 0.75; ^{1}H-NMR (DMSO-D_6, δ [ppm]): 12.32 (bs, 1H, amide-NH), 8.19 (d, 1H, ^{4}J = 2.07 Hz, naphthyl H-8), 8.01 (d, 1H, ^{3}J = 8.85 Hz, naphthyl H-5), 7.91-7.88 (m, 1H, naphthyl H-4), 7.56-7.49 (m, 3H, naphthyl H-2,3,6), 7.34-7.32 (m, 1H, aminothiazole H-4), 4.59 (s, 2H, Ar-CH_2-Ar), 4.32 (s, 2H, -CH_2-Cl); ^{13}C-NMR (DMSO-D_6, δ [ppm]): 165.13 q (amide-C), 156.67 q (aminothiazole C-2), 136.02 q (naphthyl C-1), 135.38 (aminothiazole C-4), 132.35 (naphthyl-C4a), 132.22 q (naphthyl C-8a), 132.00 q (aminothiazole C-5), 131.45 q (naphthyl C-7), 131.29 (naphthyl C-5), 128.26 (naphthyl C-2), 127.79 (naphthyl C-4), 126.81 (naphthyl C-3), 126.70 (naphthyl C-6), 123.24 (naphthyl C-8), 42.62 (-CH_2-Cl), 29.60 (Ar-CH_2-Ar); ESI-MS(-): 349.0 $[M-H]^-$

General Procedure for S-Alkylation to generate Thioethers (**13a-h**, **14a-k**, **14m-o**, **14q-r**, **19a-e**, **19g-q**, **20a**, **20c-d**, **26a-b**, **28-30**, **32**)[32] The aromatic thiol (1 equiv, 0.5 mmol) was dissolved in 2 mL of DMSO. Na_2CO_3 (2 equiv) and KI (1 equiv) were added. The mixture was stirred for 15 min at room temperature. Then, the alkyl chloride (1 equiv) was added to the reaction mixture and stirred for 2 h. After completion, water (10 mL) was added. The aqueous layer was extracted with ethyl acetate (3 x 20 mL). The combined organic layers were dried over Na_2SO_4 and evaporated. If necessary, the product was purified by automated flash column chromatography (cyclohexane/EtOAc: gradient).

N-[5-[(7-Chloro-1-naphthyl)methyl]thiazol-2-yl]-2-(4,6-dimethylpyrimidin-2-yl)sulfanyl-acetamide (**14a**): From **17f** and **33**. Yield: 66% of a beige solid; mp: 217-219 °C; R_f: 0.62; ^{1}H-NMR (DMSO-D_6, δ [ppm]): 12.20 (bs, 1H, amide-NH), 8.17 (d, 1H, ^{4}J = 2.12 Hz, naphthyl H-8), 8.00 (d, 1H, ^{3}J = 8.62 Hz, naphthyl H-5), 7.88 (dd, 1H, ^{3}J = 7.12 Hz, ^{4}J = 2.25 Hz, naphthyl H-4), 7.55-7.47 (m, 3H, naphthyl H-2,3,6), 7.30-7.28 (m, 1H, aminothiazole H-4), 6.93 (s, 1H, pyrimidine H-5), 4.56 (s, 2H, Ar-CH_2-Ar), 4.05 (s, 2H, -CH_2-S-Ar), 2.26 (s, 6H, pyrimidine -CH_3); ^{13}C-NMR (DMSO-D_6, δ [ppm]): 169.28 q (pyrimidine C-2), 167.38 q (pyrimidine C-4,6), 167.24 q (amide-C), 157.09 q (aminothiazole C-2), 136.08 q (naphthyl C-1), 135.32 (aminothiazole C-4), 132.34 q (naphthyl C-4a), 132.23 q (naphthyl C-8a), 131.41 q (aminothiazole C-5), 131.35 q (naphthyl C-7), 131.27 (naphthyl C-2), 128.23 (naphthyl C-5), 127.74 (naphthyl C-4), 126.77 (naphthyl C-6), 126.66 (naphthyl C-3), 123.24 (naphthyl C-8), 116.50 (pyrimidine C-5), 34.43 (-CH_2-S-Ar), 29.64 (Ar-CH_2-Ar), 23.61 (pyrimidine -CH_3); Purity: 99.3% (11.28 min, M2.2); ESI-MS(+): 477.1 $[M+Na]^+$

General Procedure for the Synthesis of 5-(Arylmethyl)thiazol-2-amines (**15a-f**, **16g**):[35] The aromatic amine (1 equiv, 20 mmol) was dissolved in a minimal amount of aqueous hydrochloric acid (2 M) under heating. The mixture was vigorously stirred and cooled to -5 – 0 °C. The hydrochloride partially precipitates. Then, a cooled and acidified solution of $NaNO_2$ (2.5 M, 1 equiv) was added dropwise. The reaction mixture was stirred for 10 min at -5 – 0 °C. $FeCl_3$ x 6 H_2O (3 equiv) was dissolved in a minimal amount of H_2O and added to the generated yellow colored arenediazonium chloride solution. Concentrated hydrochloric acid was given to the stirred reaction mixture until arenediazonium tetrachloroferrate(II) precipitated quantitatively. The temperature was maintained at -5 – 0 °C. The precipitated salt was filtered off and dried. A solution of $CuCl_2$ x 2 H_2O (0.5 equiv) in 23 mL of ethanol and 1.5 mL of concentrated

hydrochloric acid was added at -5 - 0 °C to a solution of the arenediazonium tetrachloroferrate(II) (1 equiv) in 30 mL of acetone. The precipitate of arenediazonium tetrachlorocuprate(II) was filtered off, washed with diethyl ether, and dried under reduced pressure. An additional amount of the salt was precipitated from the filtrate by adding 50 mL of diethyl ether. The arenediazonium tetrachlorocuprate(II) was gradually added in portions to acrolein (2.5 equiv) dissolved in 40 mL of aqueous acetone (1:1 (v/v)) while stirring at room temperature. After the evolution of nitrogen has stopped, water (50 mL) was added. Diethyl ether was added to extract the α-chloropropanal from the aqueous layer. Combined organic layers were dried over Na_2SO_4 and solvents were evaporated. The crude α-chloropropanal (1 equiv) was dissolved in ethanol (20 mL), and thiourea (1.6 g, 21 mmol) was added. The reaction mixture was heated under reflux for 2 h. After cooling to room temperature, water (100 mL) was added and the mixture was neutralized with ammonia. The aqueous layer was extracted with ethyl acetate (3 x 100 mL). The combined organic layers were dried over Na_2SO_4 and volatiles were evaporated. The brown crude product was purified by automated flash column chromatography (cyclohexane/EtOAc: gradient) to yield the aminothiazole.

5-[(7-Chloro-1-naphthyl)methyl]thiazol-2-amine (**15d**): From **21b**. Yield: 25% of a beige solid; R_f: 0.27; ^{1}H-NMR (DMSO-D_6, δ [ppm]): 8.16 (d, 1H, ^{4}J = 2.00 Hz, naphthyl H-8), 7.99 (d, 1H, ^{3}J = 8.81 Hz, naphthyl H-5), 7.88-7.84 (m, 1H, naphthyl H-4), 7.53 (dd, 1H, ^{3}J = 8.81 Hz, ^{4}J = 2.00 Hz, naphthyl H-6), 7.51-7.45 (m, 2H, naphthyl H-2,3), 6.75-6.72 (m, 1H, aminothiazole H-4), 6.69 (bs, 2H, -NH_2), 4.37 (s, 2H, -CH_2-); ^{13}C-NMR (DMSO-D_6, δ [ppm]): 168.14 q (aminothiazole C-2), 136.46 q (naphthyl C-1), 136.07 (aminothiazole C-4), 132.30 q (naphthyl C-8a), 132.28 q (naphthyl C-4a), 131.26 q (naphthyl C-7), 131.21 (naphthyl C-5), 127.92

(naphthyl C-2), 127.51 (naphthyl C-3), 126.69 (naphthyl C-6), 126.64 (naphthyl C-4), 124.63 q (aminothiazole C-5), 123.28 (naphthyl C-8), 30.16 (-CH_2-); ESI-MS(+): 275.1 $[M+H]^+$

General Procedure for the Synthesis of 5-(Arylmethyl)thiazol-2-amines (**16a-f**):[35a] The aniline derivative (1 equiv, 20 mmol) was dissolved in a minimal amount of aqueous hydrochloric acid (2 M) under heating. The mixture was vigorously stirred and cooled to -5 – 0 °C. The hydrochloride partially precipitates. Then, a cooled and acidic solution of $NaNO_2$ (2.5 M, 1 equiv) was added dropwise to the reaction mixture. The reaction mixture was incubated for 10 min at -5 – 0 °C. In the synthesis of **16b-e** the generated yellow colored arenediazonium chloride solution was preliminary neutralized with $NaHCO_3$ to a pH of 6-7, and MgO (0.25 equiv) was added to the mixture. The acidic (**16a**, **16f**) or neutralized (**16b-e)** solution of the arenediazonium chloride was added dropwise to a flask, which was loaded with acrolein (1 equiv), $CuCl_2$ x 2 H_2O (0.3 equiv), and 5 mL of acetone. The reaction mixture was stirred at room temperature until the evolution of nitrogen stopped. Then, the organic layer was separated, and the aqueous layer was extracted with diethyl ether. The organic layer was combined with the extracts, dried over Na_2SO_4, and solvents were removed under reduced pressure. The crude α-chloropropanal (1 equiv) was dissolved in ethanol (20 mL) and thiourea (1.6 g, 21 mmol) was added. The reaction mixture was heated under reflux for 2 h. After cooling to room temperature, water (100 mL) was added and the mixture was neutralized with ammonia. The aqueous layer was extracted with ethyl acetate (3 x 100 mL). The combined organic layers were dried over Na_2SO_4 and volatiles were evaporated. The brown crude product was purified by automated flash column chromatography (cyclohexane/EtOAc: gradient) to yield the aminothiazole.

5-(m-Tolylmethyl)thiazol-2-amine (**16e**): From 3-methylaniline as previously reported.[35a] Yield: 3% of a beige solid; R_f: 0.28; ^{1}H-NMR ($CDCl_3$, δ [ppm]): 7.25-7.19 (m, 1H, 3-tolyl H-5),

7.10-7.02 (m, 3H, 3-tolyl H-2,4,6), 6.82-6.78 (m, 1H, aminothiazole H-4), 5.31 (bs, 2H, $-NH_2$), 3.93 (s, 2H, Ar-CH_2-Ar), 2.36 (s, 3H, 3-tolyl -CH_3); ^{13}C-NMR ($CDCl_3$, δ [ppm]): 167.83 q (aminothiazole C-2), 139.71 q (3-tolyl C-1), 138.19 q (3-tolyl C-3), 135.31 (aminothiazole C-4), 129.10 (3-tolyl C-2), 128.43 (3-tolyl C-5), 127.76 q (aminothiazole C-5), 127.35 (3-tolyl C-4), 125.35 (3-tolyl C-6), 33.24 (Ar-CH_2-Ar), 21.37 (3-tolyl -CH_3); ESI-MS(+): 205.1 $[M+H]^+$

General Procedure for the Reduction of Nitronaphthalenes to generate Naphthalenamines (**21a-c**): The nitronaphthalene (1 equiv, 12 mmol) and $SnCl_2$ x 2 H_2O were suspended in 100 mL of ethanol. The reaction mixture was stirred for 4 - 24 h at room temperature. After completion, the solvent was evaporated, and residues were suspended in 1 L of NaOH (1 M). The product was extracted with ethyl acetate (3 x 200 mL). Combined organic layers were dried over Na_2SO_4 and evaporated under reduced pressure. The crude product was purified by automated flash column chromatography (cyclohexane/EtOAc: gradient).

7-Chloronaphthalen-1-amine (**21b**): From **23b**. Yield: 65% of a purple solid; R_f: 0.90; ^{1}H-NMR ($CDCl_3$, δ [ppm]): 7.84 (d, 1H, ^4J = 1.93 Hz, H-8), 7.76 (d, 1H, ^3J = 8.87 Hz, H-5), 7.42 (dd, 1H, ^3J = 8.87 Hz, ^4J = 1.93 Hz, H-6), 7.32-7.29 (m, 2H, H-3,4), 6.85-6.82 (m, 1H, H-2), 4.17 (bs, 2H, $-NH_2$); ^{13}C-NMR ($CDCl_3$, δ [ppm]): 141.25 q (C-1), 132.55 q (C-4a), 130.63 q (C-7), 130.09 (C-5), 126.63 (C-6), 126.57 (C-3), 124.31 q (C-8a), 120.20 (C-8), 118.83 (C-4), 110.76 (C-2); ESI-MS(-): 176.1 $[M-H]^-$

Synthesis of Nitronaphthalenamines (**22a-b**):[36] Concentrated sulfuric acid (120 mL) was cooled to -5 to -10 °C and treated slowly with 2-aminonaphthalene-1-sulfonic acid (1 equiv, 70.5 mmol) under vigorous stirring. Most of the 2-aminonaphthalene-1-sulfonic acid was soluble and the liquid was cooled to -15 °C. Dry powdered potassium nitrate (1 equiv) was added. The brown solution was stirred for 40 min at this temperature and then poured onto 0.5 kg of ice. The

precipitate was filtered off, washed, and then extracted with a cold diluted sodium carbonate solution. The filtered extracts were cooled to 5 °C and acidified with concentrated hydrochloric acid. After 2 h on ice, a mixture of mono-nitrated 2-aminonaphthalene-1-sulfonic acids was filtered off, washed with ice water, and dried. The reaction yielded 9.65g (95%) of a tan crystalline powder. Without further purification, the mixture of mono-nitrated 2-aminonaphthalene-1-sulfonic acids was suspended in 140 mL of 45% sulfuric acid and refluxed for 40 min. The hot mixture was diluted to 2 L with water and an aqueous solution of sodium hydroxide was added to a basic pH. The suspension was cooled to 10 °C for 1.5 h, and the precipitated material was filtered off, washed with water, and dried. The structural isomers were separated by automated flash column chromatography (cyclohexane/EtOAc: gradient).

8-Nitronaphthalen-2-amine (**22b**): Yield: 27% of a deep red solid; R_f: 0.86; ^{1}H-NMR (DMSO-D_6, δ [ppm]): 8.18 (dd, 1H, ^{3}J = 7.84 Hz, ^{4}J = 1.26 Hz, naphthyl H-7), 8.06-8.00 (m, 1H, naphthyl H-5), 7.80 (d, 1H, ^{3}J = 8.87 Hz, naphthyl H-4), 7.54 (d, 1H, ^{4}J = 2.29 Hz, naphthyl H-1), 7.18 (t, 1H, ^{3}J = 7.84 Hz, naphthyl H-6), 7.08 (dd, 1H, ^{3}J = 8.87 Hz, ^{4}J = 2.29 Hz, naphthyl H-3), 6.19 (s, 2H, -NH_2); ^{13}C-NMR (DMSO-D_6, δ [ppm]): 151.33 q (naphthyl C-2), 143.12 q (naphthyl C-8), 135.64 (naphthyl C-5), 130.84 (naphthyl C-4), 128.12 q (naphthyl C-4a), 127.75 q (naphthyl C-8a), 125.70 (naphthyl C-7), 119.65 (naphthyl C-3), 118.95 (naphthyl C-6), 101.12 (naphthyl C-1); ESI-MS(-): 187.1 $[M-H]^-$.

General Procedure for the Synthesis of Halonitronaphthalenes (**23a-c**):[37] The respective nitronaphthylamine (1 equiv, 32.6 mmol) was dissolved in 33 mL of glacial acid. A solution of sodium nitrite (1.7 equiv) dissolved in 33 mL of concentrated sulfuric acid was added gradually with stirring, the temperature was kept at 15-20 °C. After another 15 min, the arenediazonium salt solution was added dropwise while stirring to a solution of freshly prepared cuprous(I)

halogenide (4 equiv) dissolved in 50 mL of concentrated hydrochloric acid (for **23a-b**), or hydrobromic acid (for **23c**). After the termination of nitrogen evolution, water was added to the reaction mixture to precipitate the product quantitatively. Precipitates were filtered off, washed with aqueous NaOH (2 M) and water.

7-Chloro-1-nitro-naphthalene (**23b**): From **22b** and CuCl dissolved in concentrated hydrochloric acid. Yield: 58% of a pale yellow solid; R_f : 0.88; ^{1}H-NMR ($CDCl_3$, δ [ppm]): 8.69 (d, 1H, ^{4}J = 1.95 Hz, H-8), 8.34 (dd, 1H, ^{3}J = 7.80 Hz, ^{4}J = 1.18 Hz, H-2), 8.16-8.11 (m, 1H, H-4), 7.93 (d, 1H, ^{3}J = 8.79 Hz, H-5), 7.60 (dd, 1H, ^{3}J = 8.79 Hz, ^{4}J = 1.95 Hz, H-6), 7.59 (t, 1H, ^{3}J = 7.80 Hz, H-3); ^{13}C-NMR ($CDCl_3$, δ [ppm]): 145.39 q (C-1), 136.12 q (C-7), 134.67 (C-4), 132.55 q (C-4a), 130.08 (C-5), 128.49 (C-6), 125.74 q (C-8a), 125.27 (C-2), 124.43 (C-3), 122.52 (C-8); EI-MS(-): 207 $[M]^-$

2-Mercapto-4,6-dimethylpyrimidine (**33**)[56] as an Example for the General Procedure for the Synthesis of 2-Mercaptopyrimidines: Thiourea (1 equiv, 26 mmol) and acetylacetone (1.5 equiv) were dissolved in ethanol. During cooling and stirring, 2.5 mL of concentrated sulfuric acid were added to the flask. After 48 h of stirring at room temperature, the reaction mixture was heated to a slight boiling under reflux for 30 min. After cooling to room temperature, the yellow crystalline mass was filtered off, washed with ice-cold ethanol, and dried under reduced pressure. The yellow solid was solved in a minimal amount of water. Barium carbonate was added to a neutral reaction. The clear filtrate from the barium salts was then evaporated to dryness. The crude product was recrystallized from ethanol. Yield: 39% of a yellow solid; R_f: 0.08; ^{1}H-NMR (DMSO-D_6, δ [ppm]): 13.40 (bs, 1H, -SH), 6.62 (s, 1H, 5-H), 2,25 (s, 6H, -CH_3); ^{13}C-NMR (DMSO-D_6, δ [ppm]): 181.67 q (C-2), 164.58 q (C-4,6); 110.16 (C-5); 21,71 (-CH_3); ESI-MS(+): 141.1 $[M+H]^+$

ASSOCIATED CONTENT

Supporting Information. Experimental details, spectral data for compounds **11a**, **11c-e**, **12a-g**, **13a-h**, **14b-k**, **14m-o**, **14q-r**, **15a-c**, **15e-f**, **16a-d**, **16f-g**, **17a-e**, **17g-j**, **18a-i**, **19a-e**, **19g-q**, **20a**, **20c-d**, **21a**, **21c**, **22a**, **23a**, **23c**, **24a-b**, **25**, **26a-b**, **27-32**, **34-47,** Tables S1-2, and Figures S1-4. This material is available free of charge *via* the Internet at http://pubs.acs.org.

AUTHOR INFORMATION

Corresponding Author

* Phone: +497612034896. E-mail: manfred.jung@pharmazie.uni-freiburg.de.

Funding Sources

The studies have been supported by the Deutsche Forschungsgemeinschaft (Inhibitors: Ju295/8-1, Si868/6-1, structural work: SFB992 Medical Epigenetics, Project Z02). J. Ovádi was supported by the Hungarian National Scientific Research Fund Grants OTKA T-101039 and K-112144. J.O., W.S. and M.J. thank the COST Action CM1406 (EPIBIOCHEM) for support.

Notes

The authors declare no competing financial interest.

ABREVIATIONS USED

AMC, 7-amino-4-methylcumarin; DIPEA, *N*,*N*-diisopropylethylamine; EtOAc, ethyl acetate; ECS, extended C-site; GAPDH, glyceraldehyde-3-phosphate dehydrogenase; HEPES, 4-(2-hydroxyethyl)-1-piperazineethanesulfonic acid; hSirt2, human sirtuin2; LOO, leave one out; MOE, molecular operating environment; RMSE, root mean square error; RP, reversed phase;

SirReal, sirtuin rearranging ligands; SMILES, simplified molecular input line entry specification; ZMAL, Cbz-(acetyl)Lys-AMC;

ACKNOWLEDGMENT

We thank Karin Schmidtkunz for performing the tests for hSirt1 inhibition and Sascha Ferlaino for NMR measurements.

REFERENCES

1. de Ruijter, A. J.; van Gennip, A. H.; Caron, H. N.; Kemp, S.; van Kuilenburg, A. B. Histone deacetylases (HDACs): characterization of the classical HDAC family. *Biochem. J.* **2003,** *370*, 737-749.

2. Sauve, A. A. Sirtuin chemical mechanisms. *Biochim. Biophys. Acta* **2010,** *1804*, 1591-1603.

3. Feldman, J. L.; Baeza, J.; Denu, J. M. Activation of the protein deacetylase SIRT6 by long-chain fatty acids and widespread deacylation by mammalian sirtuins. *J. Biol. Chem.* **2013,** *288*, 31350-31356.

4. Jiang, H.; Khan, S.; Wang, Y.; Charron, G.; He, B.; Sebastian, C.; Du, J.; Kim, R.; Ge, E.; Mostoslavsky, R.; Hang, H. C.; Hao, Q.; Lin, H. SIRT6 regulates TNF-alpha secretion through hydrolysis of long-chain fatty acyl lysine. *Nature* **2013,** *496*, 110-113.

5. Du, J.; Zhou, Y.; Su, X.; Yu, J. J.; Khan, S.; Jiang, H.; Kim, J.; Woo, J.; Kim, J. H.; Choi, B. H.; He, B.; Chen, W.; Zhang, S.; Cerione, R. A.; Auwerx, J.; Hao, Q.; Lin, H. Sirt5 is a NAD-dependent protein lysine demalonylase and desuccinylase. *Science* **2011,** *334*, 806-809.

6. North, B. J.; Marshall, B. L.; Borra, M. T.; Denu, J. M.; Verdin, E. The human Sir2 ortholog, SIRT2, is an NAD^+-dependent tubulin deacetylase. *Mol. Cell* **2003,** *11*, 437-444.

7. Yeung, F.; Hoberg, J. E.; Ramsey, C. S.; Keller, M. D.; Jones, D. R.; Frye, R. A.; Mayo, M. W. Modulation of NF-kappaB-dependent transcription and cell survival by the SIRT1 deacetylase. *EMBO J.* **2004,** *23*, 2369-2380.

8. Vaziri, H.; Dessain, S. K.; Ng Eaton, E.; Imai, S. I.; Frye, R. A.; Pandita, T. K.; Guarente, L.; Weinberg, R. A. hSIR2(SIRT1) functions as an NAD-dependent p53 deacetylase. *Cell* **2001,** *107*, 149-159.

9. North, B. J.; Rosenberg, M. A.; Jeganathan, K. B.; Hafner, A. V.; Michan, S.; Dai, J.; Baker, D. J.; Cen, Y.; Wu, L. E.; Sauve, A. A.; van Deursen, J. M.; Rosenzweig, A.; Sinclair, D. A. SIRT2 induces the checkpoint kinase BubR1 to increase lifespan. *EMBO J.* **2014,** *33*, 1438-1453.

10. Du, J.; Jiang, H.; Lin, H. Investigating the ADP-ribosyltransferase activity of sirtuins with NAD analogues and ^{32}P-NAD. *Biochemistry* **2009,** *48*, 2878-2890.

11. Haigis, M. C.; Guarente, L. P. Mammalian sirtuins - emerging roles in physiology, aging, and calorie restriction. *Genes Dev.* **2006,** *20*, 2913-2921.

12. Verdin, E.; Hirschey, M. D.; Finley, L. W.; Haigis, M. C. Sirtuin regulation of mitochondria: energy production, apoptosis, and signaling. *Trends Biochem. Sci.* **2010,** *35*, 669-675.

13. Liu, T. F.; Vachharajani, V. T.; Yoza, B. K.; McCall, C. E. NAD^+-dependent sirtuin 1 and 6 proteins coordinate a switch from glucose to fatty acid oxidation during the acute inflammatory response. *J. Biol. Chem.* **2012,** *287*, 25758-25769.

14. Feige, J. N.; Auwerx, J. Transcriptional targets of sirtuins in the coordination of mammalian physiology. *Curr. Opin. Cell Biol.* **2008,** *20*, 303-309.

15. Schemies, J.; Uciechowska, U.; Sippl, W.; Jung, M. NAD(+) -dependent histone deacetylases (sirtuins) as novel therapeutic targets. *Med. Res. Rev.* **2010,** *30*, 861-889.

16. Beirowski, B.; Gustin, J.; Armour, S. M.; Yamamoto, H.; Viader, A.; North, B. J.; Michan, S.; Baloh, R. H.; Golden, J. P.; Schmidt, R. E.; Sinclair, D. A.; Auwerx, J.; Milbrandt, J. Sir-two-homolog 2 (Sirt2) modulates peripheral myelination through polarity protein Par-3/atypical protein kinase C (aPKC) signaling. *Proc. Natl. Acad. Sci. U S A* **2011,** *108*, E952-961.

17. de Oliveira, R. M.; Sarkander, J.; Kazantsev, A. G.; Outeiro, T. F. SIRT2 as a therapeutic target for age-related disorders. *Front. Pharmacol.* **2012,** *3*, 82.

18. (a) Pais, T. F.; Szego, E. M.; Marques, O.; Miller-Fleming, L.; Antas, P.; Guerreiro, P.; de Oliveira, R. M.; Kasapoglu, B.; Outeiro, T. F. The NAD-dependent deacetylase sirtuin 2 is a suppressor of microglial activation and brain inflammation. *EMBO J.* **2013,** *32*, 2603-2616; (b) Zhao, T.; Alam, H. B.; Liu, B.; Bronson, R. T.; Nikolian, V. C.; Wu, E.; Chong, W.; Li, Y. Selective inhibition of SIRT2 improves outcomes in a lethal septic model. *Curr. Mol. Med.* **2015,** *15,* 634-641; (c) Eskandarian, H. A.; Impens, F.; Nahori, M. A.; Soubigou, G.; Coppee, J. Y.; Cossart, P.; Hamon, M. A. A role for SIRT2-dependent histone H3K18 deacetylation in bacterial infection. *Science* **2013,** *341*, 1238858.

19. (a) Kim, H. S.; Vassilopoulos, A.; Wang, R. H.; Lahusen, T.; Xiao, Z.; Xu, X.; Li, C.; Veenstra, T. D.; Li, B.; Yu, H.; Ji, J.; Wang, X. W.; Park, S. H.; Cha, Y. I.; Gius, D.; Deng, C. X. SIRT2 maintains genome integrity and suppresses tumorigenesis through regulating APC/C activity. *Cancer Cell* **2011,** *20*, 487-499; (b) Yang, M. H.; Laurent, G.; Bause, A. S.; Spang, R.; German, N.; Haigis, M. C.; Haigis, K. M. HDAC6 and SIRT2 regulate the acetylation state and oncogenic activity of mutant K-RAS. *Mol. Cancer Res.* **2013,** *11*, 1072-1077.

20. Donmez, G.; Outeiro, T. F. SIRT1 and SIRT2: emerging targets in neurodegeneration. *EMBO Mol. Med.* **2013,** *5*, 344-352.

21. Park, S. H.; Zhu, Y.; Ozden, O.; Kim, H. S.; Jiang, H.; Deng, C. X.; Gius, D.; Vassilopoulos, A. SIRT2 is a tumor suppressor that connects aging, acetylome, cell cycle signaling, and carcinogenesis. *Transl. Cancer Re.s* **2012,** *1*, 15-21.

22. Lawson, M.; Uciechowska, U.; Schemies, J.; Rumpf, T.; Jung, M.; Sippl, W. Inhibitors to understand molecular mechanisms of NAD(+)-dependent deacetylases (sirtuins). *Biochim. Biophys. Acta* **2010,** *1799*, 726-739.

23. Cui, H.; Kamal, Z.; Ai, T.; Xu, Y.; More, S. S.; Wilson, D. J.; Chen, L. Discovery of potent and selective sirtuin 2 (SIRT2) inhibitors using a fragment-based approach. *J. Med. Chem.* **2014,** *57*, 8340-8357.

24. Suzuki, T.; Khan, M. N. A.; Sawada, H.; Imai, E.; Itoh, Y.; Yamatsuta, K.; Tokuda, N.; Takeuchi, J.; Seko, T.; Nakagawa, H.; Miyata, N. Design, synthesis, and biological activity of a novel series of human sirtuin-2-selective inhibitors. *J. Med. Chem.* **2012,** *55*, 5760-5773.

25. Disch, J. S.; Evindar, G.; Chiu, C. H.; Blum, C. A.; Dai, H.; Jin, L.; Schuman, E.; Lind, K. E.; Belyanskaya, S. L.; Deng, J.; Coppo, F.; Aquilani, L.; Graybill, T. L.; Cuozzo, J. W.; Lavu, S.; Mao, C.; Vlasuk, G. P.; Perni, R. B. Discovery of thieno[3,2-d]pyrimidine-6-carboxamides as potent inhibitors of SIRT1, SIRT2, and SIRT3. *J. Med. Chem.* **2013,** *56*, 3666-3679.

26. Di Fruscia, P.; Zacharioudakis, E.; Liu, C.; Moniot, S.; Laohasinnarong, S.; Khongkow, M.; Harrison, I. F.; Koltsida, K.; Reynolds, C. R.; Schmidtkunz, K.; Jung, M.; Chapman, K. L.; Steegborn, C.; Dexter, D. T.; Sternberg, M. J. E.; Lam, E. W. F.; Fuchter, M. J. The Discovery of a highly selective 5,6,7,8-tetrahydrobenzo[4,5]thieno[2,3-d] pyrimidin-4(3H)-one SIRT2 inhibitor that is neuroprotective in an in vitro Parkinson's disease model. *ChemMedChem* **2015,** *10*, 69-82.

27. Outeiro, T. F.; Kontopoulos, E.; Altmann, S. M.; Kufareva, I.; Strathearn, K. E.; Amore, A. M.; Volk, C. B.; Maxwell, M. M.; Rochet, J. C.; McLean, P. J.; Young, A. B.; Abagyan, R.; Feany, M. B.; Hyman, B. T.; Kazantsev, A. G. Sirtuin 2 inhibitors rescue alpha-synuclein-mediated toxicity in models of Parkinson's disease. *Science* **2007,** *317*, 516-519.

28. (a) Lara, E.; Mai, A.; Calvanese, V.; Altucci, L.; Lopez-Nieva, P.; Martinez-Chantar, M. L.; Varela-Rey, M.; Rotili, D.; Nebbioso, A.; Ropero, S.; Montoya, G.; Oyarzabal, J.; Velasco, S.; Serrano, M.; Witt, M.; Villar-Garea, A.; Imhof, A.; Mato, J. M.; Esteller, M.; Fraga, M. F. Salermide, a Sirtuin inhibitor with a strong cancer-specific proapoptotic effect. *Oncogene* **2009,** *28*, 781-791; (b) Peck, B.; Chen, C. Y.; Ho, K. K.; Di Fruscia, P.; Myatt, S. S.; Coombes, R. C.; Fuchter, M. J.; Hsiao, C. D.; Lam, E. W. SIRT inhibitors induce cell death and p53 acetylation through targeting both SIRT1 and SIRT2. *Mol. Cancer Ther.* **2010,** *9*, 844-55.

29. Yamagata, K.; Goto, Y.; Nishimasu, H.; Morimoto, J.; Ishitani, R.; Dohmae, N.; Takeda, N.; Nagai, R.; Komuro, I.; Suga, H.; Nureki, O. Structural basis for potent inhibition of SIRT2 deacetylase by a macrocyclic peptide inducing dynamic structural change. *Structure* **2014,** *22*, 345-352.

30. Rumpf, T.; Schiedel, M.; Karaman, B.; Roessler, C.; North, B. J.; Lehotzky, A.; Olah, J.; Ladwein, K. I.; Schmidtkunz, K.; Gajer, M.; Pannek, M.; Steegborn, C.; Sinclair, D. A.; Gerhardt, S.; Ovadi, J.; Schutkowski, M.; Sippl, W.; Einsle, O.; Jung, M. Selective Sirt2 inhibition by ligand-induced rearrangement of the active site. *Nat. Commun.* **2015,** *6*, 6263.

31. Chubb, F. L.; Nissenbaum, J. Some Hypoglycemic Thiadiazoles. *Can. J. Chem.* **1959,** *37*, 1121-1123.

32. Zav'yalov, S. I.; Kravchenko, N. E.; Ezhova, G. I.; Kulikova, L. B.; Zavozin, A. G.; Dorofeeva, O. V. Synthesis of 2-aminothiazole derivatives. *Pharm. Chem. J.* **2007,** *41*, 105-108.

33. Meerwein, H.; Büchner, E.; van Emster, K. Über die Einwirkung aromatischer Diazoverbindungen auf α, β-ungesättigte Carbonylverbindungen. *J. Prakt. Chem.* **1939,** *152*, 237-266.

34. Bülow, C.; Sproesser, T. Über primäre Disazokombinationen des Benzyläthyl-m-amidophenols. *Ber. Dtsch. Chem. Ges.* **1908,** *41*, 1684-1692.

35. (a) Obushak, N. D.; Matiichuk, V. S.; Vasylyshin, R. Y.; Ostapyuk, Y. V. Heterocyclic syntheses on the basis of arylation products of unsaturated compounds: X. 3-aryl.-2-chloropropanals as reagents for the synthesis of 2-amino-1,3-thiazole derivatives. *Russ. J. Org. Chem.* **2004,** *40*, 383-389; (b) Obushak, N. D.; Lyakhovich, M. B.; Bilaya, E. E. Arenediazonium

tetrachlorocuprates(II). Modified versions of the Meerwein and Sandmeyer reactions. *Russ. J. Org. Chem.* **2002,** *38*, 38-46.

36. Morrison, D. C.; Lee, H. P. C. A new preparation of 8-Nitro-2-Naphthylamine. *J. Org. Chem.* **1962,** *27*, 3336-3337.

37. Beech, W. F.; Legg, N. Aminohydroxynaphthoic acids .1. Synthesis of 6-amino-4-hydroxy-2-naphthoic acid (carboxy gamma-acid). *J. Chem. Soc.* **1949,** 1887-1889.

38. Heltweg, B.; Trapp, J.; Jung, M. In vitro assays for the determination of histone deacetylase activity. *Methods* **2005,** *36*, 332-337.

39. Kazantsev, A. G. Compositions and methods for modulating sirtuin activity, and therapeutic use. U.S. Patent No. 20090259044, **2012.**

40. Neugebauer, R. C.; Uchiechowska, U.; Meier, R.; Hruby, H.; Valkov, V.; Verdin, E.; Sippl, W.; Jung, M. Structure-activity studies on splitomicin derivatives as sirtuin inhibitors and computational prediction of binding mode. *J. Med. Chem.* **2008,** *51*, 1203-1213.

41. North, B. J.; Schwer, B.; Ahuja, N.; Marshall, B.; Verdin, E. Preparation of enzymatically active recombinant class III protein deacetylases. *Methods* **2005,** *36*, 338-345.

42. Kabsch, W., Xds. *Acta Crystallogr., Sect. D: Biol. Crystallogr.* **2010,** *66*, 125-132.

43. Karplus, P. A.; Diederichs, K. Linking crystallographic model and data quality. *Science* **2012,** *336*, 1030-1033.

44. Winn, M. D.; Ballard, C. C.; Cowtan, K. D.; Dodson, E. J.; Emsley, P.; Evans, P. R.; Keegan, R. M.; Krissinel, E. B.; Leslie, A. G. W.; McCoy, A.; McNicholas, S. J.; Murshudov, G.

N.; Pannu, N. S.; Potterton, E. A.; Powell, H. R.; Read, R. J.; Vagin, A.; Wilson, K. S. Overview of the CCP4 suite and current developments. *Acta Crystallogr., Sect. D: Biol. Crystallogr.* **2011,** *67*, 235-242.

45. Vagin, A.; Teplyakov, A. Molecular replacement with MOLREP. *Acta Crystallogr., Sect. D: Biol. Crystallogr.* **2010,** *66*, 22-25.

46. Emsley, P.; Lohkamp, B.; Scott, W. G.; Cowtan, K. Features and development of Coot. *Acta Crystallogr., Sect. D: Biol. Crystallogr.* **2010,** *66*, 486-501.

47. Murshudov, G. N.; Skubak, P.; Lebedev, A. A.; Pannu, N. S.; Steiner, R. A.; Nicholls, R. A.; Winn, M. D.; Long, F.; Vagin, A. A. REFMAC5 for the refinement of macromolecular crystal structures. *Acta Crystallogr., Sect. D: Biol. Crystallogr.* **2011,** *67*, 355-367.

48. Chen, V. B.; Arendall, W. B.; Headd, J. J.; Keedy, D. A.; Immormino, R. M.; Kapral, G. J.; Murray, L. W.; Richardson, J. S.; Richardson, D. C. MolProbity: all-atom structure validation for macromolecular crystallography. *Acta Crystallogr., Sect. D: Biol. Crystallogr.* **2010,** *66*, 12-21.

49. Laskowski, R. A.; Macarthur, M. W.; Moss, D. S.; Thornton, J. M. Procheck - a Program to Check the Stereochemical Quality of Protein Structures. *J. Appl. Crystallogr.* **1993,** *26*, 283-291.

50. Adams, P. D.; Afonine, P. V.; Bunkoczi, G.; Chen, V. B.; Davis, I. W.; Echols, N.; Headd, J. J.; Hung, L. W.; Kapral, G. J.; Grosse-Kunstleve, R. W.; McCoy, A. J.; Moriarty, N. W.; Oeffner, R.; Read, R. J.; Richardson, D. C.; Richardson, J. S.; Terwilliger, T. C.; Zwart, P.

H. PHENIX: a comprehensive Python-based system for macromolecular structure solution. *Acta Crystallogr., Sect. D: Biol. Crystallogr.* **2010,** *66*, 213-221.

51. Krissinel, E. Fold Recognition Using Efficient Short Fragment Clustering. *J. Mol. Biochem.* **2012**, *1*, 76-85

52. Brunger, A. T. Free R-value - a novel statistical quantity for assessing the accuracy of crystal-structures. *Nature* **1992,** *355*, 472-475.

53. Wang, J. M.; Wolf, R. M.; Caldwell, J. W.; Kollman, P. A.; Case, D. A. Development and testing of a general amber force field. *J. Comput. Chem.* **2004,** *25*, 1157-1174.

54. Jakalian, A.; Jack, D. B.; Bayly, C. I. Fast, efficient generation of high-quality atomic charges. AM1-BCC model: II. Parameterization and validation. *J. Comput. Chem.* **2002,** *23*, 1623-1641.

55. Slynko, I.; Scharfe, M.; Rumpf, T.; Eib, J.; Metzger, E.; Schüle, R.; Jung, M.; Sippl, W. Virtual screening of PRK1 inhibitors: Ensemble docking, rescoring using binding free energy calculation and QSAR model development. *J. Chem. Inf. Model* **2014,** *54*, 138-150.

56. Hale, W. J.; Williams, A. G. The constitution of acetylacetone-thiourea. *J. Am. Chem. Soc.* **1915,** *37*, 594-600.

57. Tan, T. F.; Li, Y. X.; Bai, L. G.; Wu, B. P.; Guo, H. Y.; Suo, Z. C. A facile synthesis and optical properties of novel 2-substituted-5-naphthylmethylene thiadiazole derivatives. *Adv. Mater. Res-Switz.* **2014,** *1052*, 188-192.

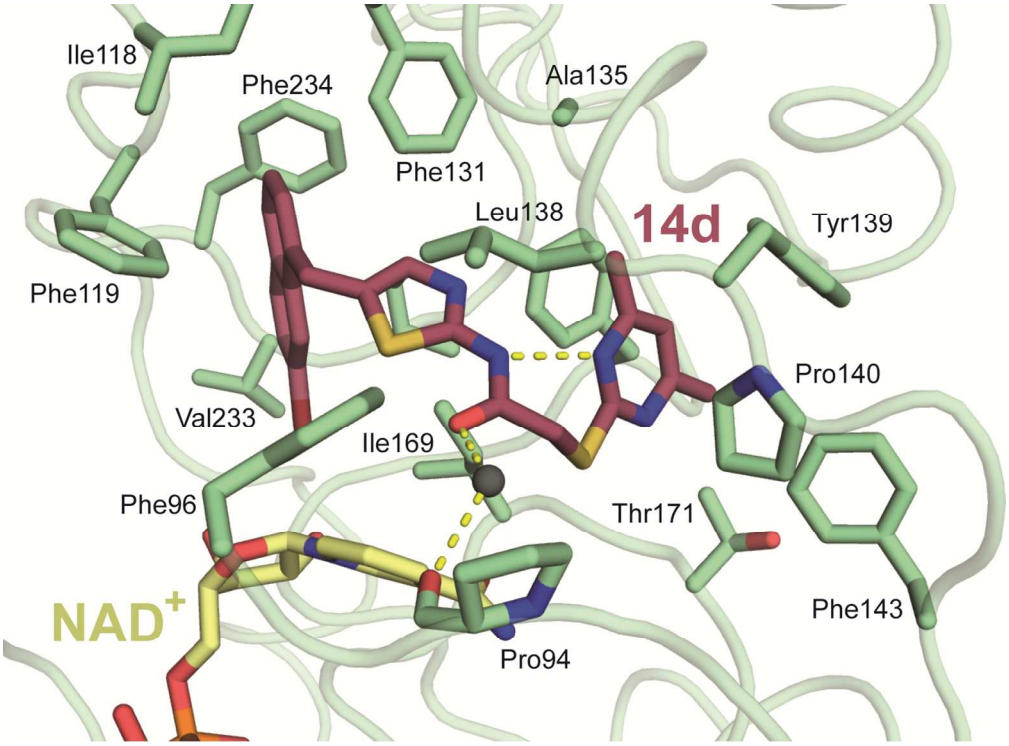
Ile118
Phe234
Ala135
Phe131
Leu138
14d
Tyr139
Phe119
Pro140
Val233
Ile169
Phe96
Thr171
NAD+
Phe143
Pro94